

# RSC Advances



This is an *Accepted Manuscript*, which has been through the Royal Society of Chemistry peer review process and has been accepted for publication.

*Accepted Manuscripts* are published online shortly after acceptance, before technical editing, formatting and proof reading. Using this free service, authors can make their results available to the community, in citable form, before we publish the edited article. This *Accepted Manuscript* will be replaced by the edited, formatted and paginated article as soon as this is available.

You can find more information about *Accepted Manuscripts* in the [Information for Authors](#).

Please note that technical editing may introduce minor changes to the text and/or graphics, which may alter content. The journal's standard [Terms & Conditions](#) and the [Ethical guidelines](#) still apply. In no event shall the Royal Society of Chemistry be held responsible for any errors or omissions in this *Accepted Manuscript* or any consequences arising from the use of any information it contains.

# Combined Experimental and Computational Insights into Key Features of L-Alanine L-Alaninium Picrate Monohydrate: Growth, Structural, Electronic and Nonlinear Optical Properties

Shabbir Muhammad<sup>a,c\*</sup>, Mohd. Shkir<sup>a,c\*</sup>, S. AlFaify<sup>a,c</sup>, Ahmad Irfan<sup>b,c</sup>, Abdullah G. Al-Sehemi<sup>b,c</sup>

<sup>a</sup>Department of Physics, College of Science, King Khalid University, Abha 61413, P.O. Box 9004, Saudi Arabia

<sup>b</sup>Department of Chemistry, Faculty of Science, King Khalid University, Abha 61413, P.O. Box 9004, Saudi Arabia

<sup>c</sup>Research Center for Advanced Materials Science (RCAMS), King Khalid University, Abha 61413, P.O. Box 9004, Saudi Arabia

## Abstract

In current work, we spotlight the novel key features of L-alanine L-alaninium picrate monohydrate (LALAPM) using a dual approach comprising of experimental and computational techniques. The single crystals of LALAPM have been grown indigenously in three different ratios (1:1, 1:5, 2:1) through slow cooling technique. The formation of different types of crystals were recorded during the growth process and found to vary significantly from each other. The grown crystals were subjected to single crystal powder X-ray diffraction analyses to confirm their respective crystal structures. Additionally, ultraviolet-visible-near infrared, diffuse reflectance measurements and optical parameter analyses were performed. The state-of-art computational techniques are used to get the ground state molecular geometry of LALAPM at B3LYP/6-31G\* level of theory. Different important electro-optical parameters (complementary to experimental results) including IR, Raman, and UV-Visible spectra have been calculated at the same level of theory. The polarizability and first hyperpolarizability (both static and dynamic) were calculated to see the potential applications of LALAPM in nonlinear optics. Furthermore, several novel molecular level insights have been obtained in the form of total and

partial density of states, HOMO-LUMO gap and electrostatic potential maps etc. The obtained quantum chemical findings are compared with experimental results. The static and frequency dependent dynamic first hyperpolarizability values of LALAPM molecule are found to be  $8.06 \times 10^{-30}$  and  $10.24 \times 10^{-30}$  esu that are about 37 times and 59 times larger than those of the prototype urea molecule, respectively, at the same B3LYP/6-31G\* level of theory. The obtained results indicate that the titled compound contains good nonlinear optical properties and can be treated as a good contender for optoelectronic device fabrications.

**Keywords:** *Crystal growth, Optical properties; Optical spectroscopy; Density functional theory*

*Corresponding author\**

*Dr. Mohd. Shkir*

*Assistant Professor*

*College of Science*

*King Khalid University, Abha, Saudi Arabia*

*E-mail: [shkirphysics@gmail.com](mailto:shkirphysics@gmail.com), [mshabbir@kku.edu.sa](mailto:mshabbir@kku.edu.sa)*

*Contact: Office: +966 530683673, Fax: +966 7 241 8319, +91 9911769335*

## **1. Introduction**

The field of linear and nonlinear optics has got a significant momentum since the discovery of photon as the fastest carrier of information. Over the past few decades, several types of materials have been functionalized to match the demand of functional materials with efficient optical and nonlinear optical (NLO) properties.<sup>1, 2</sup> Organic materials are excellent candidates for hi-tech laser applications due to their fast and giant nonlinear response over an extensive frequency range, inherent synthetic flexibility and large optical damage threshold for laser power and low frequency dispersion. One of the key advantages of these organic materials is that they permit one to modify the chemical structure with large physical structural diversity and properties for the desired NLO properties.<sup>3-9</sup> The optical single crystals being used as devices for high optical data storage, frequency converter, fusion research etc. So it is very important to grow new as

well as existing optical single crystals with high perfection for devices fabrication because of such needful applications. Crystals of amino acid family are of great interest due to their attractive nonlinear optical properties.<sup>10-12</sup> When an organic acid mixed with amino acid, usually its nonlinear optical property increases due to the zwitterionic nature associated with enhanced transparency range.<sup>13, 14</sup> Picric acid is an organic acid and forms molecular charge transfer complexes with aromatic compounds through electrostatic or hydrogen bonding interactions,<sup>15, 16</sup> and has many reports with many organic molecules with interesting properties,<sup>17-20</sup> due to the presence of active  $\pi$  and ionic bonds.<sup>21</sup>

The picric acid and L-alanine are good NLO materials that show excellent NLO efficiency better than that of KDP.<sup>22-25</sup> These compounds also have a good tendency to form a new compound by reacting with each other as well as with other organic and inorganic materials such as diglycine picrate, L-leucine L-leucinium picrate,<sup>6, 18, 26, 27</sup>  $\beta$ -alanine  $\beta$ -alaninium picrate,<sup>28</sup> 2-aminopyridinium picrate,<sup>4, 29</sup> DL-phenylalanine DL-phenylalaninium picrate,<sup>30</sup> DL-methionine DL-methioninium picrate<sup>31</sup>. Furthermore investigations of these crystals were also carried out in some previous studies,<sup>32, 33</sup> including DL-valine DL-valinium picrate<sup>34</sup> etc. Salts of amino acids are an interesting class from different points of view i.e. as species with very short hydrogen bonds, crystals in which phase transitions are possible, due to presence of dimeric cations as well as many of them are nonlinear optical materials. There are more than 20 new salts that have been recently reported with dimeric cations.<sup>35</sup>

Recently, along the above lines for picrate compounds, Ghazaryan et al.,<sup>36</sup> have reported the L-alanine L-alaninium picrate. They have obtained the single crystals of L-alanine L-alaninium picrate monohydrate. They have also performed IR and single crystal analyses of L-alanine +

picric acid + H<sub>2</sub>O system and characterized the final product as L-alanine L-alaninium picrate system with two more phases and revisited the previous findings on L-alanine + picric acid + H<sub>2</sub>O system.<sup>37</sup> Very recently, another experimental study was performed to highlight the nucleation kinetics, growth and hardness parameters of LALAPM.<sup>38</sup>

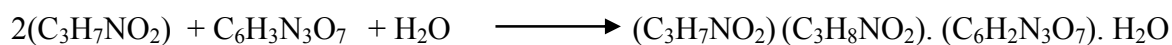
The above recent reports specify the preliminary experimental findings about LALAPM. Nevertheless, the first use of a dual approach comprising of experimental and computational techniques will spotlight the several novel features of LALAPM including its geometrical parameters, configuration of frontier molecular orbitals (FMOs) as well as its nonlinear optical properties, which are still not known to scientific community. For instance, the corner stone of the present investigation is to provide molecular level insights to explore the potential of LALAPM for advanced functional materials in the framework of combined computational and experimental investigations. Furthermore, bulk crystal growth by slow cooling technique, morphology, optical analysis using UV-Vis-NIR and diffuse reflectance (DR) will be performed. Thus the aims of present investigation are manifold. The growth of L-alanine L-alaninium picrate monohydrate (LALAPM) single crystals is done using slow cooling technique in three different ratios and subsequently the indigenously grown single crystals are subjected to the single crystal and powder X-ray diffraction analysis. During the single crystals growth process, their morphology is also recorded randomly by inverted microscope. The grown crystals were subjected to UV-vis-NIR spectroscopy measurements. Additionally, the molecular geometry optimization and calculation of electro-optical properties have been performed using different advanced theoretical methods to shed light on bonding features among L-alanine, L-alaninium, picric acid and water molecules. The IR, Raman and UV-Visible spectra, polarizability, first hyperpolarizability are calculated using DFT, TD-DFT and finite field (FF) methods,

respectively. The obtained computational and experimental results are discussed and compared with each other wherever possible.

## 2. Experimental and Computational Details

### 2.1. Synthesis, solubility and crystal growth

For synthesis of the titled compound, L-alanine and picric acid of high purity were purchased from Loba Chemie Pvt. Ltd. and has been taken in different ratios such as 1:1, 1.5:1 and 2:1 and mixed in double distilled water. The calculated amounts of the both materials were weighed by an electronic balance (METTLER TOLEDO) of high accuracy and taken into three good quality borosil glass beakers. For complete dissolving, homogenization and proper chemical reaction of all three materials, it was stirred well at a temperature of 38 °C with the help of a Eurotherm temperature controlled magnetic stirrer. Finally, all the prepared solutions were kept at room temperature and allowed to evaporate to yield the yellow crystalline powder salt of LALAPM of three different ratios. The chemical reaction of LALAPM (2:1) formation is given below:



L-alanine            picric acid    water                            L-alanine L-alaninium picricrate monohydrate

Before going for crystal growth of titled material it is very important to study its solubility. Therefore we have determined the solubility curve of LALAPM using deionized water as a solvent in the temperature range of 28–58 °C. Gravimetric method<sup>39</sup> was used to calculate the required amount of LALAPM which will be added to saturate the aqueous solution at 28 °C and we have repeated this process for different temperatures. The solubility curve is represented in Figure 1 (a) and found in close agreement with earlier report<sup>38</sup>. LALAPM shows the positive solubility-temperature gradient in an aqueous solution and it is a positive point for growing the bulk crystals. From its solubility curve it is clear that the titled material is highly soluble in water

hence it will be easy to grow the bulk single crystals of LALAPM from the solution technique. The bulk growth of L-alanine L-alaninium picrate monohydrate (LALAPM) was done by slow cooling technique. For the growth of single crystals of LALAPM, the saturated solution of all the synthesized ratios were prepared above the room temperature i.e. 32 °C using double distilled water with continuous stirring for more than 2 days to get the homogeneous and transparent solution of yellow color.

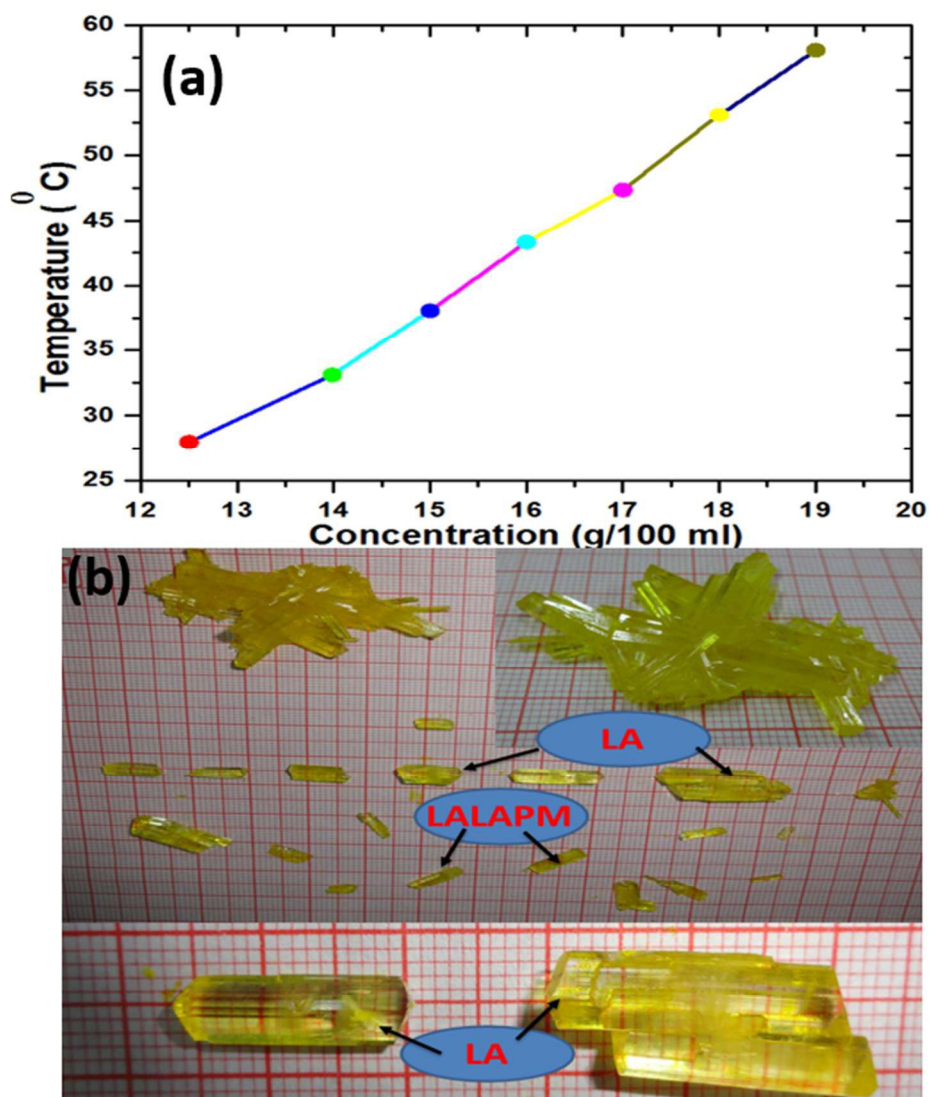


**Figure 1** (a) solubility curve and (b) grown single crystals of LALAPM and LA from similar solution (2:1)

The prepared solutions were filtered in three other beakers, covered with a perforated lid and kept in a constant temperature bath (CTB) at the same prepared temperature having the temperature accuracy of  $\pm 0.01^\circ\text{C}$  and left for one day. After one day, we have started to reduce the temperature of CTB by  $0.5^\circ\text{C}/\text{day}$  for slow cooling and during this the solutions were watched by inverted microscope the nucleation was started in all the beakers after four days when the temperature reach to  $30^\circ$ . We have reduced the temperature reduction rate to  $0.1^\circ\text{C}$  for further growth. Good quality, large size and different shapes single crystals were harvested from the mother solutions after a span of 20 days as shown in Figure 1(b), which were confirmed and found to be of large size L-alanine (contained picric acid) as well as comparatively small size LALAPM, as it was also mentioned by Ghazaryan et al. in their recently published article on the titled compound. The well-known floatation method was applied to determine the density of the grown crystal using a liquid-mixture of bromoform and carbon tetrachloride and found to be  $1.5168\text{ g cm}^{-3}$  which is in good agreement with the reported value i.e.  $1.517\text{ g cm}^{-3}$ <sup>36</sup> and warrant that the grown crystal is of LALAPM.

## 2.2. Characterization

The morphology of the growing crystals for all three solutions was randomly recorded with the help of inverted microscope made by Motic, which interfaced with computer system. The pictures were captured using a camera (Moticam 2300, 3.0M pixel USB 2.0) attached with microscope. The objective lens of magnification PH 10X/0.25,  $\infty/1.1\text{WD}7.5$  was used in our experiment for the present investigation. The random morphology of growing crystals is shown in Figure 2 and indicates that there are different types of crystal formations happening including L-alanine (with/without modified morphology due to the addition of picric acid)<sup>40, 41</sup> and

LALAPM in the same solution.<sup>42</sup> These crystals can be also matched with grown crystals as shown in Figure 1(b).

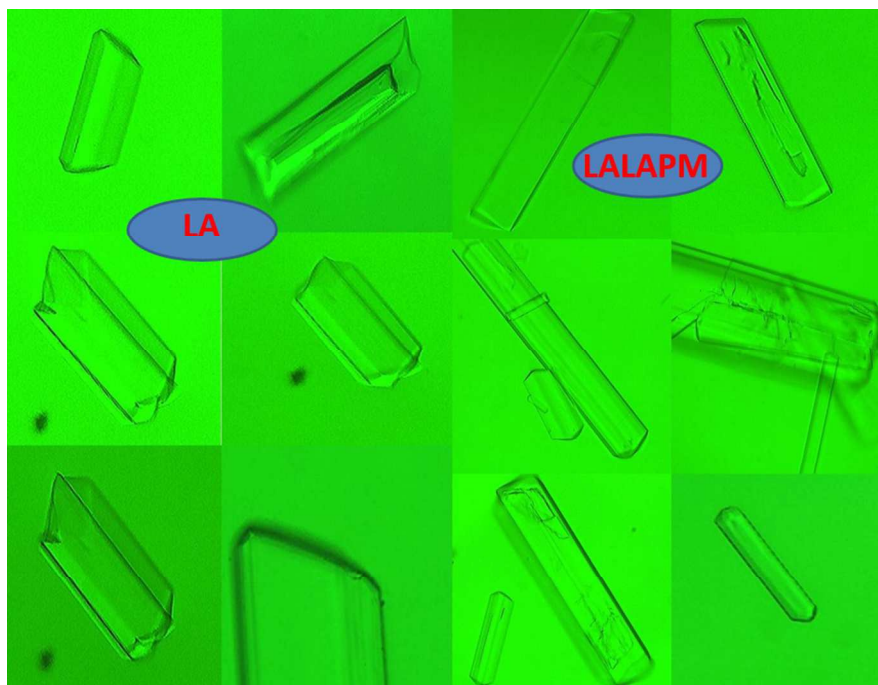


**Figure 2** Randomly recorded morphologies of LALAPM (2:1) solution

To confirm the crystal system and lattice parameters of grown crystals, their single crystal X-ray diffraction analyses were performed. Single crystals of suitable size (0.17 x 0.20 x 0.45 mm) were cut from a larger specimen. The crystal structure was confirmed by using the intensity data collected using a Bruker Kappa Apex II diffractometer (graphite-monochromated,  $\text{MoK}_\alpha = 0.71073\text{\AA}$ ) at 296 K. The least-squares refinement of the diffraction angles of 25 reflections was done to obtain the cell data. For further confirmation of crystal system and determine the lattice parameters of both type of grown single crystals, they were crushed into fine powder of size  $\sim 150\mu\text{m}$  and subjected to PW3710 based Philips Analytical Powder X-ray diffractometer with

nickel filtered, CuK $\alpha$  radiation operated at 35 kV, 30mA and the scanning was done in step size 0.02° in the angular range 5-70° of 2-theta.

To calculate the various optical parameters of LALAPM single crystal and LA crystal (for comparison), their optical absorbance were recorded in the wavelength range of 200-800 nm at 300K by using a JASCO V-570 UV-vis-NIR spectrophotometer. A shimadzu UV-VIS-NIR spectrophotometer model (UV-3600) was used to record the diffuse reflectance (DR) in the wavelength range from 230-2300 nm of the powdered sample of the grown crystals with an attachment of integrating sphere.

### 2.3. Computational details

All the calculations have been performed using Gaussian suit of programs.<sup>43</sup> The molecular geometry of LALAPM was optimized by density functional theory (DFT) using B3LYP/6-31G\* level of theory. In addition to B3LYP, highly correlated method MP2 and recently developed M06 functional have also applied to optimized initial geometry for comparison of results with B3LYP and experiment. The equilibrium geometry of LALAPM was successfully achieved corresponding to the true minimum on the potential energy surface (PES) by solving self-consistent field equation. The optimized structural parameters of LALAPM were used to characterize all stationary points as minima using IR and Raman frequency calculations. The IR and Raman spectra of LALAPM were calculated by taking the second derivative of the energy that is computed analytically. Similarly, all other electronic properties including UV-Visible spectra, dipole moment, polarizability, first hyperpolarizability of LALAPM were calculated at the same level of theory. The time dependent density functional theory (TD-DFT) has been used to calculate excitation energies with relatively larger basis set of 6-31+G\*. The static first hyperpolarizability ( $\beta_{\text{tot}}$ ) and its components for LALAPM were calculated by finite field (FF)

method. The FF method has been broadly applied to investigate the NLO properties of organic materials because this methodology can be used in concert with the electronic structure method to calculate  $\beta$  values. Recently, several  $\beta_{\text{tot}}$  amplitudes calculated by this method are found to be in a semi quantitative agreement with experimental structure property relationship.<sup>8, 44</sup> In FF method, a molecule is subjected to a static electric field ( $F$ ), the energy ( $E$ ) of the molecule is expressed by the following equation:

$$E = E^{(0)} - \mu_1 F_1 - \frac{1}{2} \alpha_{ij} F_i F_j - \frac{1}{6} \beta_{ijk} F_i F_j F_k - \frac{1}{24} \gamma_{ijkl} F_i F_j F_k F_l - \quad (1)$$

where  $E^{(0)}$  is the energy of molecule in the absence of an electric field,  $\mu$  is the components of the dipole moment vector,  $\alpha$  is the linear polarizability,  $\beta$  and  $\gamma$  are the first and second hyperpolarizabilities, respectively, while  $i, j$  and  $k$  label the  $x, y$  and  $z$  components respectively. It is clear from the above equation that the values of  $\mu$ ,  $\alpha$ ,  $\beta$ , and  $\gamma$  can be obtained by differentiating  $E$  with respect to  $F$ . Furthermore the chemical hardness ( $\eta$ ) of LALAPM molecule has been calculated by using its HOMO and LUMO energy values. These parameters of the titled compound were obtained by using Koopman's theorem<sup>45</sup> for closed-shell molecules, the chemical hardness of any molecule can be calculated by the following relation (An approximation for absolute hardness  $\eta$  was developed earlier<sup>46-48</sup>) as given below:

$$\eta = \frac{I-A}{2} \quad (2)$$

where  $A$  ( $= -E_{\text{HOMO}}$ ) is the ionization potential and  $I$  ( $= -E_{\text{LUMO}}$ ) is the electron affinity of the molecule. The values of  $A$  and  $I$  of LALAPM were calculated by B3LYP/6-31G\* level of theory.

### 3. Results and Discussion

#### 3.1. Single crystal and powder X-ray diffraction (PXRD) studies

Single crystal and powder X-ray diffraction (PXRD) analysis were done for the confirmation of crystal system, space group, lattice parameters of LALAPM as well as L-Alanine and compared with the reported values.<sup>36, 49</sup> Recorded PXRD data was used as input for calculating the lattice parameters by using different software's like 'CHECKCELL',<sup>50</sup> and 'POWDERX',<sup>6, 50</sup> from the obtained results it was confirmed that the grown crystals of LALAPM belongs to Monoclinic crystal system with space group of  $P2_1$  and the determined unit cell parameters by single crystal XRD as well as refined by above said software and the reported one are listed in Table 1. The calculated parameters were found in good agreement with the earlier reported data<sup>36</sup>.

**Table 1** Lattice parameters of LALAPM crystals.

Lattice parameters	Reported work		Present work (LALAPM)		
	L-alanine <sup>52</sup>	LALAPM <sup>36</sup>	Single crystal XRD data	Powder XRD refined data by POWDERX	Powder XRD refined data by CHECKCELL
a	5.784(1) Å	8.268(2) Å	8.268(5) Å	8.29811 Å	8.2345 Å
b	6.032(1) Å	7.510(2) Å	7.510(6) Å	7.51048 Å	7.5696 Å
c	12.343(1) Å	15.540(3) Å	15.540(4) Å	15.60090 Å	15.5254 Å
V	430.636 Å <sup>3</sup>	931.0(3) Å <sup>3</sup>	931.0 Å <sup>3</sup>	936.749 Å <sup>3</sup>	937.243 Å <sup>3</sup>
$\alpha$	90	90°	90°	90°	90°
$\beta$	90	105.23°	105.23°	105.540°	104.42°
$\gamma$	90	90°	90°	90°	90°
System	orthorhombic	monoclinic	monoclinic	monoclinic	monoclinic
S.G	$P2_12_12_1$	$P2_1$	$P2_1$	$P2_1$	$P2_1$

#### 3.2. Molecular geometry analysis

The initial molecular geometry of LALAPM molecule has been extracted from single crystal data<sup>42</sup> and subjected to full optimization at three different levels of theory including B3LYP/6-31G\*, M06/6-31G\* and MP2/6-31G\* as collected in Table 2 (labeling is according to Figure 3). The important bond parameters have collected in Table 2 and experimentally reported values are also given for comparison.<sup>42</sup> Overall there is reasonable agreement among bond lengths at different levels of theory as well as with experimental bond values except hydrogen bonds involving H<sub>2</sub>O molecule, which perhaps has not well-defined position in its experimental structure. In present study, the optimized unit contains one picrate anion, one zwitterionic L-alanine and one L-alaninium cation. The hydrogen bond between zwitterionic L-alanine and L-alaninium cation is about 1.727 Å near to 1.70 Å of its experimental value. The dimeric distance between O<sub>1</sub>-O<sub>3</sub> is about 2.498 Å, which also in a semi-quantitative agreement with its experimental value of 2.553 Å as seen from Table 3.

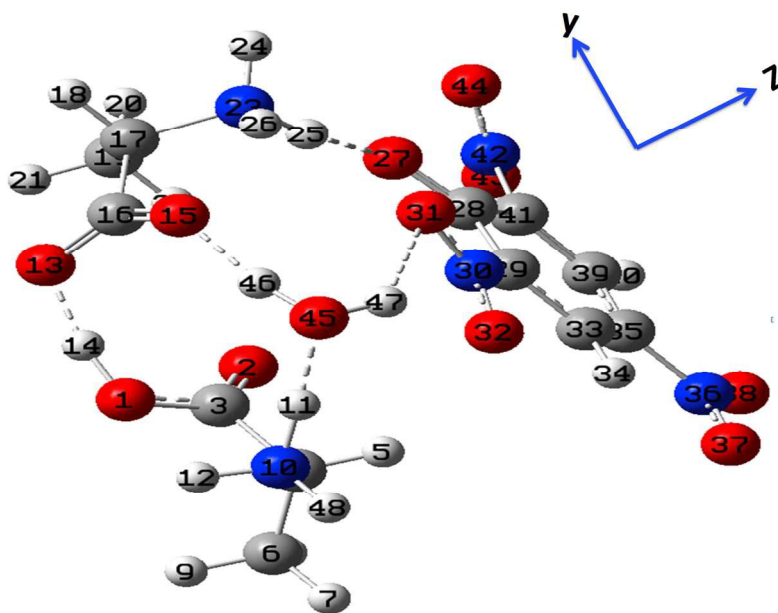


**Figure 3** The optimized structure of LALAPM monohydrate at B3LYP/6-31G\* level of theory and white, red, gray and blue atoms represent H, O, C, N atoms, respectively.

The nitro (NO<sub>2</sub>) groups of picrate ion are slightly out of the plan with their torsion angles of 122°, 124° and 125° like as in usual picrate molecule. The H<sub>2</sub>O molecule is held between zwitterionic L-alanine and one L-alaninium cation and picrate anion through hydrogen bonds. The water molecule forms one hydrogen bond with picrate anion while two hydrogen bonds with L-alanine and L-alaninium molecules. The water molecule can be envisaged as connecting bridge among L-alanine, L-alaninium cation and picrate anion through hydrogen bonding.

**Table 2** The bond lengths [Å] and bond angles [°] of optimized LALAPM molecule at different functionals with 6-31G\* basis set

Bond lengths	Exp. [36]	Cal.			Bond Angles	Exp. [36]	Cal.		
		B3LYP	M06	MP2			B3LYP	M06	MP2
O1-O13	2.553	2.498	2.489	2.518	O1-O3-O2	125.96	125.65	128.167	128.02
C16-O13	1.255	1.257	1.253	1.264	O13-C16-O15	125.65	128.86	128.77	128.97
C16-O15	1.258	1.238	1.251	1.264	O13-C16-C17	112.43	115.15	115.59	115.86
C28-O27	1.255	1.247	1.237	1.262	C16-C17-N23	107.8	105.14	105.36	105.18
C41-N42	1.466	1.447	1.463	1.459	O27-C28-C29	123.47	125.85	125.65	127.68
O15-O45	2.836	2.718	2.723	2.723	C29-C28-C41	112.24	112.351	112.10	111.46
H14...O13	1.703	1.727	1.446	1.459	C28-C41-C39	124.85	124.06	124.25	125.79
H11...O45	1.948	1.493	1.545	1.544	O1-H14-O13	171.00	169.51	167.45	168.64
H46...O15	2.01	1.743	1.763	1.760	O31-N30-O32	120.67	122.19	120.95	121.17
H47...O32	2.09	2.04	2.03	2.024	O37-N36-O38	123.97	124.40	124.62	124.41
H25...O27	1.950	1.638	1.657	1.634	O44-N42-O43	121.03	124.66	124.91	125.49

### 3.2. IR and Raman Spectroscopic Analysis

Vibrational spectroscopic study is a highly effective tool in identifying the functional groups present in any molecule as well as in molecular conformational and in analysis of reaction

kinetics<sup>51</sup>. The vibrational spectra (IR and Raman) of LALAPM molecule were determined using B3LYP/6-31G\* level of theory as shown in Figure 4(a) and 4(b), respectively. It is well known that due to the combination of electron correlation effects and basis set deficiencies calculated harmonic frequencies are found to be higher than the experimentally observed frequencies. Notwithstanding with the level of calculations, it is usual to scale down the calculated harmonic frequencies in order to develop the covenant with experimental values. The scaled frequencies minimize the root mean square difference between calculated and experimental frequencies for bands with definite identifications. All the observed wavenumbers and their corresponding assignments along with the experimentally reported assignments are listed in Table 3. From Figure 4, it is clear that there are characteristic vibrations in the titled molecule due to presence of zwitterionic L-alanine and L-alaninium moieties as well as picrate anion and water molecule<sup>36</sup>. It is expected that the stretching vibrations of OH bonds of water molecules, N-H and C-H bonds of the NH<sub>3</sub> and CH<sub>3</sub> and CH groups of alanine and alaninium moieties as well as C-H bonds in the picrate anions are expected in the high-frequency region. The graphical presentation of some main vibrations such as O-H, N-H, C-H, C-C, CH<sub>3</sub>, NO<sub>2</sub> are shown in Figure 5. Because of strong hydrogen bonding O-H...O in the dimeric cation absorption due to stretching vibration of O-H bonds in L-alaninium moieties is not expected in high frequency region<sup>36</sup>.

The O-H stretching vibrations of crystallization water are assigned for absorption bands observed at ~3499 and 3386, 3308 cm<sup>-1</sup> and respective Raman-bands. While experimentally these bands are observed at 3570, 3416 in IR and 3567 and 3423 in Raman<sup>36</sup>. The above assigned bands positions are in accordance with relatively weak hydrogen bonds formed by water molecule (see Figure 5). The bands observed in IR and Raman spectra both below 3300 cm<sup>-1</sup> are mainly caused

by hydrogen bonded symmetric and asymmetric stretching of  $\text{NH}_3$  groups, respectively (see Figure 5). The peaks observed at  $\sim 3054, 3028, 3011, 2960, 2942 \text{ cm}^{-1}$  in Raman and  $2954, 2936 \text{ cm}^{-1}$  in IR are assigned to C-H stretching vibrations (see Figure 5). While experimentally these bands were observed at  $2943$  in IR and  $2982, 2971, 2950$  in Raman <sup>36</sup>. The bands observed at  $\sim 2730, 2175, 2054, 1760 \text{ cm}^{-1}$  in IR and  $\sim 2725, 2180, 2080, 1763 \text{ cm}^{-1}$  in Raman spectra are assigned as sum tones, these bands are well correlated with earlier report <sup>36</sup>.

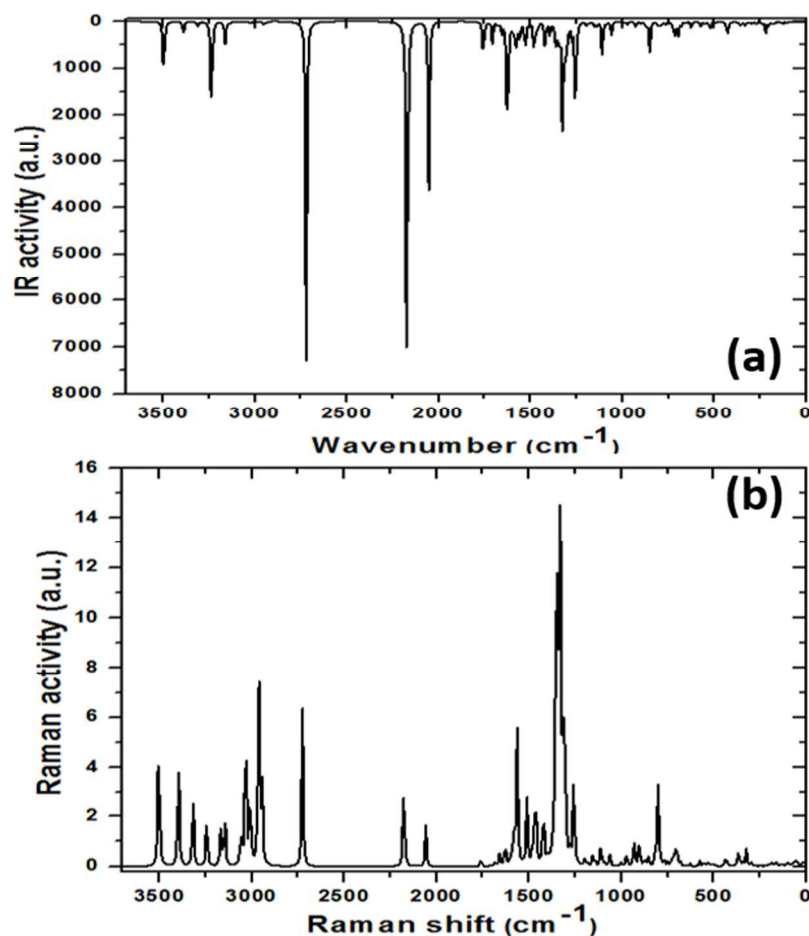


**Figure 4** Calculated (a) IR and (b) Raman spectra of LALAPM molecule at B3LYP/6-31G\* level of theory

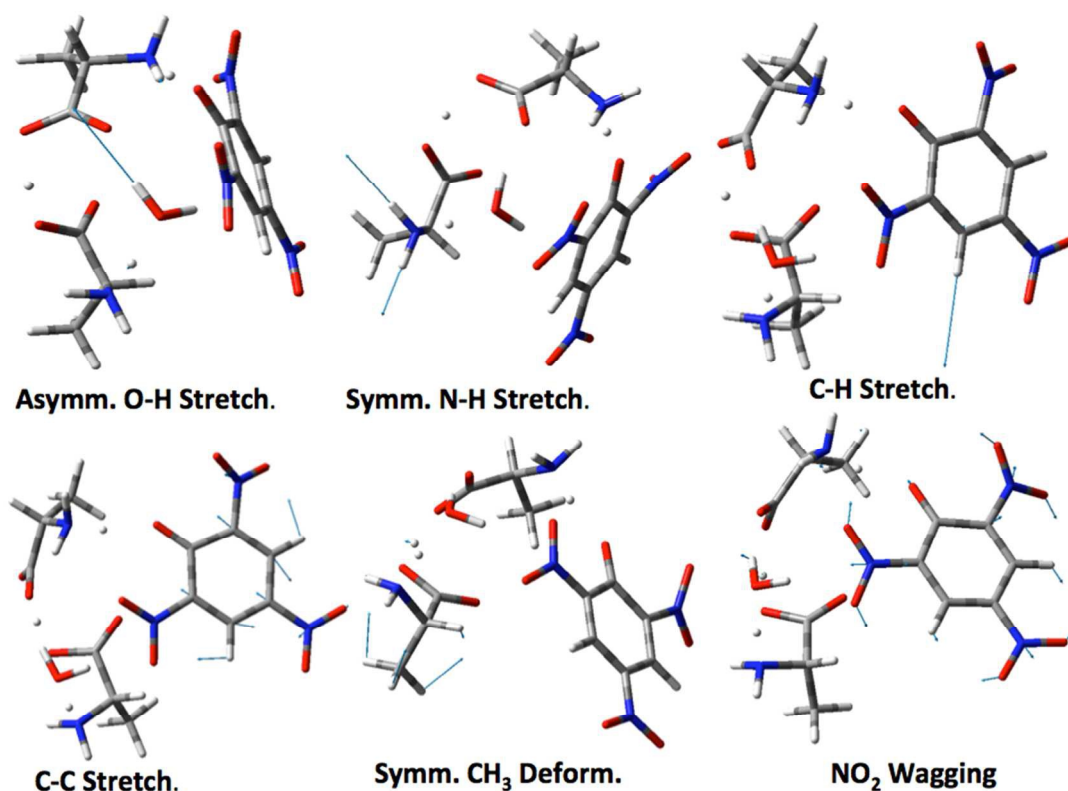


**Figure 5.** The pictorial representation of vibrational modes with their displacement vectors (light blue arrows) at B3LYP/6-31G\* level of theory

Now, we discuss the bands observed below  $1800\text{ cm}^{-1}$ . The absorption band at  $\sim 1708\text{ cm}^{-1}$  in IR and respective Raman-band at  $1685\text{ cm}^{-1}$  are assigned to stretching vibration of C=O bond in COOH group. While these bands observed experimentally at 1703 and 1702 respectively in IR and Raman<sup>36</sup>. In the range of  $1650\text{--}1400\text{ cm}^{-1}$  several characteristic bands are expected due to picrate anion. The peaks at  $\sim 1656, 1630\text{ cm}^{-1}$  in IR and  $1659, 1628\text{ cm}^{-1}$  in Raman spectra are assigned to C=C ring stretching (see Figure 5), asymmetric stretching and deformation of  $\text{COO}^-$  and  $\text{NH}_3^+$  vibrations. While these bands observed experimentally at 1633, 1614 and 1634, 1611 respectively in IR and Raman<sup>36</sup>. The bands at  $1578\text{ cm}^{-1}$  in IR and  $1580\text{ cm}^{-1}$  in Raman are assigned to  $\text{NH}_3^+$  bending vibration. Bands at  $\sim 1561, 1526\text{ cm}^{-1}$  in IR and  $1564\text{ cm}^{-1}$  in Raman spectra are assigned to asymmetric vibration and deformation of  $\text{NO}_2$  and  $\text{NH}_3^+$  respectively.

While these bands observed experimentally at 1566, 1539 and 1554  $\text{cm}^{-1}$ , respectively in IR and Raman <sup>36</sup>. The band at 1483  $\text{cm}^{-1}$  and 1512  $\text{cm}^{-1}$  in IR and Raman are assigned to symmetric deformation of  $\text{NH}_3^+$  vibration. While these bands at 1501, 1490 and 1554  $\text{cm}^{-1}$ , respectively are observed experimentally in IR and Raman <sup>36</sup>. The band at  $\sim 1460 \text{ cm}^{-1}$  in Raman is assigned to asymmetric deformation of  $\text{CH}_3$  vibration. However, experimentally this band is found in both IR and Raman at 1478, 1458 and 1467 respectively <sup>36</sup>. The bands observed at 1422  $\text{cm}^{-1}$  and 1420  $\text{cm}^{-1}$  are assigned to symmetric vibration of  $\text{COO}^-$  group. While experimentally only in IR this band is observed at 1429 <sup>36</sup>. The bands at  $\sim 1396, 1362 \text{ cm}^{-1}$  in IR and 1350  $\text{cm}^{-1}$  in Raman are assigned to asymmetric deformation of  $\text{CH}_3$  vibration (see Figure 5). While these bands are observed experimentally at 1384, 1366 and 167  $\text{cm}^{-1}$ , respectively in IR and Raman <sup>36</sup>. The most intensive peaks in the Raman spectrum at 1327, 1330, 1312, and 801  $\text{cm}^{-1}$  and respective peaks in the IR spectrum are assigned to vibrations of nitro groups. While these bands are observed experimentally at 1340, 1332 and 825  $\text{cm}^{-1}$  in Raman and respective in IR <sup>36</sup>. This group has characteristic vibrations active in IR and Raman spectra both. The band at 1275, 1258  $\text{cm}^{-1}$  in IR and 1260  $\text{cm}^{-1}$  in Raman are assigned to C=O phenolic and C-OH vibrations, respectively. While these bands are observed at 1299, 1260 and 1301, 1271  $\text{cm}^{-1}$ , respectively in IR and Raman experimentally <sup>36</sup>. The band observed at 1197, 1180, 1154  $\text{cm}^{-1}$  and 1200, 1156  $\text{cm}^{-1}$  are assigned to in plane deformation of CH group. While these bands are observed at 1194, 1163 and 1169, 1147  $\text{cm}^{-1}$ , respectively in IR and Raman experimentally <sup>36</sup>. The bands at 1137, 1111  $\text{cm}^{-1}$  in IR and 1115  $\text{cm}^{-1}$  in Raman are assigned to  $\rho(\text{NH}_3^+)$ , while these bands experimentally are observed at 1118 and 1123  $\text{cm}^{-1}$ , respectively, 1065, 972  $\text{cm}^{-1}$  and 1065, 1000, 975  $\text{cm}^{-1}$  in IR and Raman spectra are assigned to CN group vibration, while these bands experimentally are observed at 1083, 1003 and 1085, 1010, 992  $\text{cm}^{-1}$ , respectively.

**Table 3** The calculated IR and Raman frequencies at B3LYP/6-31G\* level of theory and experimentally reported IR and Raman frequencies with their appropriate assignments for LALAPM

IR frequencies ( $\text{Cm}^{-1}$ )		Raman frequencies ( $\text{cm}^{-1}$ )		Assignments
Calculated	Experimental [29]	Calculated	Experimental [29]	
3499	3570	3505	3567	OH ( $\text{H}_2\text{O}$ ) Asymmetric stretching
3386,3308	3416	3393,3314	3423	OH ( $\text{H}_2\text{O}$ ) symmetric stretching
3239	3192	3245	3210	NH( $\text{NH}_3^+$ ) Asymmetric stretching
3161	3104	3167,3141	3104	NH( $\text{NH}_3^+$ ) Symmetric stretching
-----	-----	3054,3028,3011	3000	CH(CH) stretching vibration
2954,2936	2943	2960,2942	2982,2971,2950	CH( $\text{CH}_3$ ) stretching vibration
2730	2730,2603,2546	2725	2748,2606	Sum tones
2175,2054	1934,1884	2180,2080	2258	Sum tones
1760	1837	1763	1839	Sum tones
1708	1703	1685	1702	C=O( $\text{COOH}$ ) stretching
1656	1633	1659	1634	vibration
1630	1614	1628	1611	$\nu(\text{C}=\text{C})$ ring; $\nu_{\text{as}}(\text{COO}^-)$
1578	-----	1580	1558	$\nu(\text{C}=\text{C})$ ring; $\delta_{\text{as}}(\text{NH}_3^+)$
1561,1526	1566,1539	1564	1554	$\nu_{\text{as}}(\text{NO}_2)$ ; $\delta_{\text{as}}(\text{NH}_3^+)$
1483	1501,1490	1512	1493	$\delta_{\text{s}}(\text{NH}_3^+)$
----	1478,1458	1460	1467	$\delta_{\text{as}}(\text{CH}_3)$
1422	1429	1420	-----	$\nu_{\text{s}}(\text{COO}^-)$
1396, 1362	1384,1366	1350	1367	$\delta_{\text{s}}(\text{CH}_3)$
1327	1340,1321	1330,1312	1334,1318	$\nu_{\text{s}}(\text{NO}_2)$
1275,1258	1299,1260	1260	1301,1271	$\nu(\text{C}-\text{O})$ phenolic; $\nu(\text{C}-\text{OH})$
1197,1180,1154	1194,1163	1200,1156	1169,1147	$\delta(\text{CH})$ in plane
1137, 1111	1118	1115	1123	$\rho(\text{NH}_3^+)$
1065	1083	1065	1085	$\nu(\text{CN})$
972	1003	1000,975	1010,992	$\nu(\text{CN})$
930	946	931	949	-----
905	915	910	920	$\rho(\text{CH}_3)$
851	844	850	846	$\nu(\text{C}-\text{C})$
----	821	801	825	$\delta(\text{NO}_2)$
799	790,772	----	793	$\delta(\text{CH})$ out-of- plane
765,747	746	750	764,751	$\omega(\text{NO}_2)$
713	712,696	706	721,698	$\delta(\text{COO}^-)$
695,678,652,626	656,618	670,630	676,660,622	-----
574	552	575	555	-----
522	529,514	532	530,517	$\rho(\text{NO}_2)$
427	472	437	427	$\rho(\text{COO}^-)$
358	Not mentioned	367	400,380,361	skelatal deformation
332	Not mentioned	324	338	-----
298	Not mentioned	300	302,276	-----
272	Not mentioned	185	203	lattice vibrations
220	Not mentioned	160	164	-----
124	Not mentioned	99,56,13	----	-----

The band at  $905\text{ cm}^{-1}$  and  $910\text{ cm}^{-1}$  are due to  $\rho(\text{CH}_3)$ ,  $851, 850\text{ cm}^{-1}$  are due to  $\nu(\text{C-C})$ ,  $801\text{ cm}^{-1}$  due to  $\delta(\text{NO}_2)$ ,  $799\text{ cm}^{-1}$  is due to  $\delta(\text{CH})$  out-of- plane,  $765, 747\text{ cm}^{-1}$  and  $750\text{ cm}^{-1}$  is due to  $w(\text{NO}_2)$  (see Figure 5), while these bands experimentally are observed at  $746$  and  $764, 751$ , respectively,  $713\text{ cm}^{-1}$  and  $706\text{ cm}^{-1}$  is due to  $\delta(\text{COO}^-)$ ,  $522\text{ cm}^{-1}$  and  $532\text{ cm}^{-1}$  are due to  $\rho(\text{NO}_2)$ ,  $427\text{ cm}^{-1}$  and  $437\text{ cm}^{-1}$  are due to  $\rho(\text{COO}^-)$  vibrations. The bands observed below  $400\text{ cm}^{-1}$  are assigned to skeletal and lattice vibrations in the molecule. All the vibrations approve the confirmation of LALAPM and agreed well with the experimental values<sup>36</sup>.

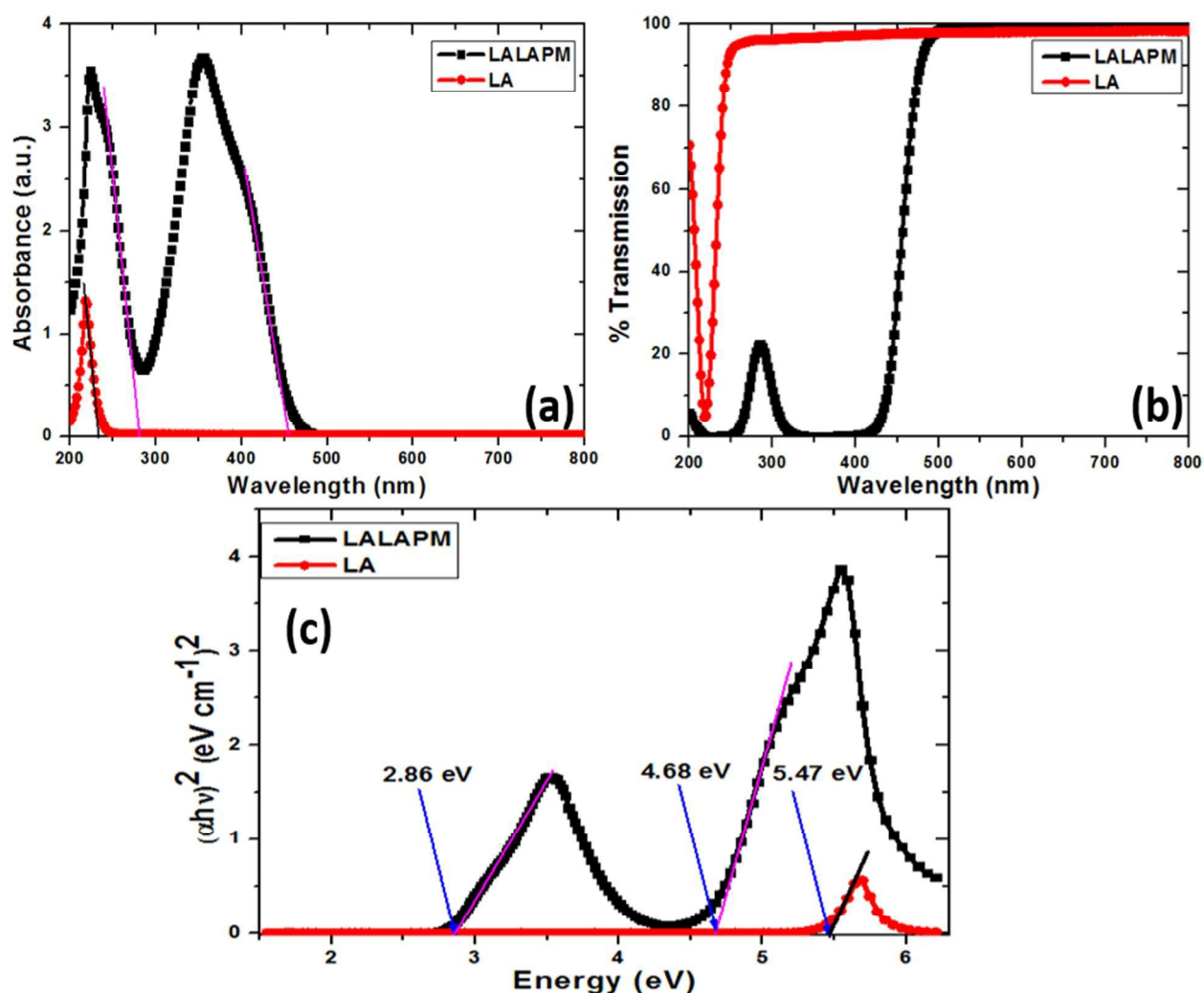


**Figure 6** UV-Vis-NIR (a) absorbance (b) transmittance and (c) band gap plots of LA and LALAPM crystals

### 3.3. Optical analysis

#### 3.3.1. UV-Vis-NIR spectroscopic study

To recognize the suitability of the grown single crystal of LALAPM for optical applications the optical light absorbance is a very essential factor to be assessed. The optical absorption spectra of the grown single crystals of L-alanine and LALAPM were recorded in the wavelengths range of 200-800 nm as shown in Figure 6(a). The optical transmission was calculated from absorption data, which shows that the grown crystals are highly transparent in the entire testing range as shown in Figure 6(b). The lower cut-off wavelength of LA was observed at ~230 nm while for LALAPM two cut-off wavelengths were observed at 286 and ~435 nm, respectively. The high percentage of transmission in the entire tested region (from 450 to 800 nm) is an essential requirement for optically active materials. The transparency of the titled compound can be compared with other reported picrate, organic, metal-organic as well as L-alanine compounds.<sup>4-7, 18, 52-61</sup>

The TD-DFT is considered to be a reliable quantum chemical technique for studying the UV-Visible absorption spectra (corresponds to vertical electronic transitions) of different organic compounds.<sup>62-64</sup> For LALAPM molecule, different TD-DFT methods (TD-B3LYP, TD-PBE0, TD-M06, TD-CAM-B3LYP and TD-B2PLYPD) have been applied to study its excitation energies on its ground state geometry, which is optimized at B3LYP/6-31G\* level of theory. The experimental electronic absorption spectrum of title crystal is showing two bands at 286 and 435 nm [6(a)]. The UV-Visible absorption spectra of LALAPM at different five TD-DFT methods with 6-31+G\* basis set have been shown in Figure 7. It can be seen from Figure 7 that all the TD-DFT methods (except TD-CAM-B3LYP) have reasonably reproduced two absorption bands as observed in its experimental absorption spectrum. For TD-CAM-B3LYP, it is already well-

known to reproduce excitation energies with long-range charge transfer effect that is not the situation in titled compound. Among all the five TD-DFT methods, the excitation energies calculated at TD-B3LYP are closer to the experimental values. The two predicted electronic absorption wavelengths are 312 and 414 nm with their oscillator strengths ( $f_0$ ) of 0.133 and 0.066 at TD-B3LYP/6-31+G\* level of theory, which are in reasonably good agreement with experimental values of 286 and 435 nm. Calculations of optimized molecular orbital geometry of LALAPM show that the visible absorption maxima is of the electron transition between frontier orbitals such as transition from HOMO to LUMO which will be explained in section 3.6. The lower energy visible band observed 435 nm (Exp.) and 414 nm (Theor.) could be attributed to the redistribution of electronic intramolecular charge involving  $\pi - \pi^*$  transitions.

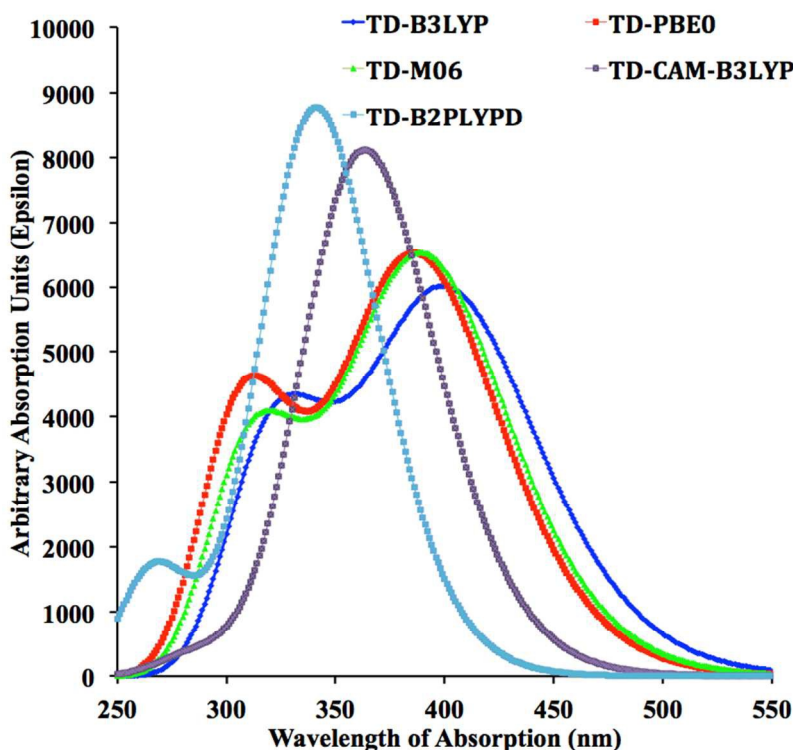


**Figure 7** Calculated UV-VIS spectra of LALAPM molecule with different TD-DFT functionals and 6-31+G\* basis set

### 3.3.2. Band gap analysis

Investigation on optical band gap of any material is a very important parameter to get deep perception about their optical recital and application in optoelectronic devices. So, the understanding of optical processes is an important factor in design and optimization of devices.

The optical band gap of the titled compound was calculated by using the optical absorption data of LA and LALAPM crystals. Initially, the optical absorption coefficient was calculated for both the crystals from the absorbance using the following relation:

$$\alpha_{crys} = 2.303 \frac{\text{Absorbance } (A_{crys})}{\text{thickness of the crystal } (t_{crys})} \quad (3)$$

$(E_g)_{crys}$  was calculated from the optical absorption coefficient  $\alpha_{crys}$  near the absorption edge according to following general relation:

$$(\Delta h\nu)^{\frac{1}{s}} = A [h\nu - (E_g)_{crys}] \quad (4)$$

where  $A$  is a constant,  $h$  is the plank's constant,  $\nu$  is the frequency of incident photon. The process of optical absorption is explained by the value of an index indicated as  $s$  in the above relation. For direct allowed, indirect allowed, indirect forbidden and direct forbidden transitions the values of  $s$  are corresponds to 1/2, 2, 3 or 3/2, respectively.

when  $s=1/2$ , which is assigned to direct allowed transition then the equation will be:

$$(\alpha h\nu)^2 = A [h\nu - (E_g)_{crys}] \quad (5)$$

The  $(E_g)_{crys}$  of LA and LALAPM single crystals was calculated by extrapolating the straight line to the x-axis ( $h\nu$ ) as shown in Figure 6(c). The band gap of LA was found to be 5.47 eV, while the LALAPM having two band gaps ~2.86 and 4.68 eV, respectively. Because of the large

band gap of the grown crystal it can be a suitable applicant for optoelectronic applications<sup>53, 59, 65-67</sup>.

### 3.3.3. Frontier Molecular Orbital (FMO) Analysis

The frontier molecular orbitals (FMOs) play a crucial role in the reactivity of any molecule. Among FMOs, the highest occupied molecular orbital (HOMO) and lowest unoccupied molecular orbital (LUMO) are very important. These FMOs of a molecule determine the way that it interacts with other species. For LALAPM molecule, its calculated energy gaps between HOMO and LUMO (HOMO-1 and LUMO+1) orbitals are 3.517 (4.943 eV), which are in semi-quantitatively agreement to experimental band gap values of 2.86 (4.68 eV), respectively. The HOMO and LUMO (H-L) energy gap describes the chemical reactivity, kinetic stability and chemical softness of a molecule. According to softness-hardness rule, molecules with larger energy gaps are known as hard molecules and they usually possess higher thermal and kinetic stabilities. Based on its H-L energy gap of LALAPM molecule, its chemical hardness value is found to be 1.758 eV, which indicates that LALAPM has significant kinetic stability (see Table 4). As the H-L energy gap is relatively larger and the transition energy exists in U.V. and near visible region, which give an advantage of significant transparency.

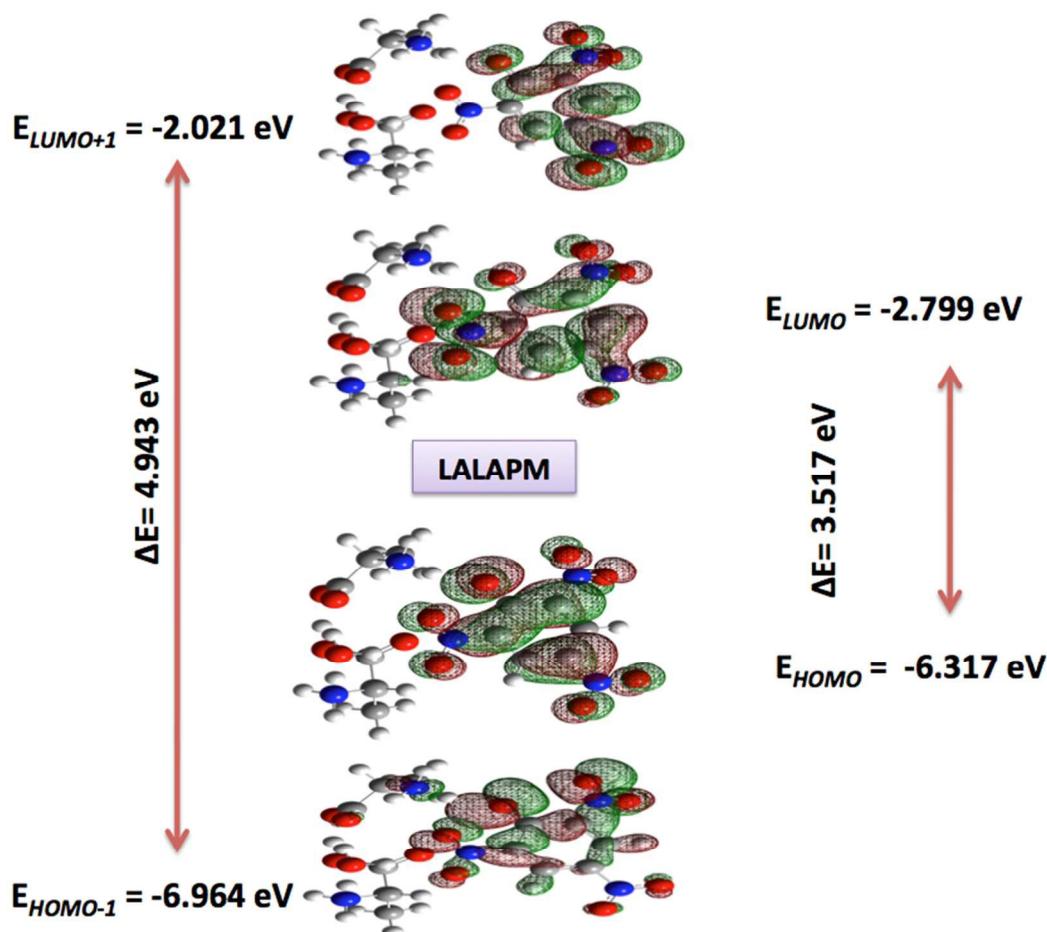


**Figure 8** The 3-D plot of frontier molecular orbitals of LALAPM molecule with counter values of  $\pm 0.02$  a. u.

In present study, the experimental UV-Visible spectrum has shown two maximum absorption wavelengths i.e. 435 and 286 nm, which are reasonably well reproduced as 414 and 312 nm at TD-B3LYP/6-31G\* level of theory, respectively. The TD-DFT calculations on LALAPM molecule show that lower energy electronic transition corresponds to the transition of electron from ground state to first excited state with HOMO to LUMO major orbital contributions (67% configuration interaction) and second transition involves HOMO to LUMO+1 major orbital contributions (43% configuration interaction). The three-dimensional plots of FMOs including HOMO, HOMO-1, LUMO, and LUMO+1 orbitals have been shown in Figure 8. From the

Figure 8, it can be seen that the HOMO and LUMO orbitals are mainly located on picrate ion, which is also evident from the DOS graph. It can be seen that the electronic density is redistributed on picrate ion during transition, which perhaps cause the non-zero amplitude of first hyperpolarizability. According to the composition of second transition, a somewhat similar pattern of charge redistribution can also be seen for HOMO and LUMO+1 orbitals, which are involved in second transition with relatively higher energy.

**Table 4** The calculated energy values of frontier molecular orbitals (FMOs) and their orbital energy gaps at B3LYP/6-31G\* level of theory for LALAPM

Orbital	eV
$E_{\text{HOMO}}$	-6.317
$E_{\text{HOMO-1}}$	-6.964
$E_{\text{LUMO}}$	-2.799
$E_{\text{LUMO+1}}$	-2.021
$\Delta E_{\text{HOMO-LUMO}}$	3.517
$\Delta E_{\text{HOMO-1-LUMO+1}}$	4.943

<sup>a</sup> 1 a. u. of energy = 27.211396 eV

### 3.3.4. Density of states

The total density of states (TDOS) and partial density of states (PDOS) are investigated for LALAPM molecule using AOMix wave function analysis program.<sup>68</sup> The TDOS and PDOS are calculated to understand the role of individual molecular fragments into the bonding and electro-optical properties of LALAPM molecule. We generate the TDOS and PDOS plots by dividing LALAPM molecule into four fragments including L-alanine, L-alaninium, picrate ion and water molecule fragments as shown in Figure 9. The TDOS and PDOS plots shows population analysis per orbital and demonstrate the modest view of the makeup of the molecular orbitals in a certain energy range while PDOS plot shows percentage contribution of each group to each molecular orbital in the final molecule. A careful analysis of Figure 9 shows that picrate anion contributes

more to the total number of states per interval of energy as compared with other fragments. The most of the high energy occupied states and lower energy unoccupied states around the band gap are composed of picrate anion fragment. Similarly the contribution of L-alaninium is significant over energy range of -6 to -7 eV and a further significant contribution is at relatively lower energy levels around -10 to -11 eV. Additionally, it can be seen that the contributions of L-alanine and water are smallest as compared to other fragments of picrate anion and L-alaninium cations. Thus, from the DOS diagram, it can be observed that the picrate anion is main fragment in LALAPM molecule that has significant influence on its electro-optical and nonlinear optical properties because any change at picrate anion fragment will significantly influence the frontier orbitals (as evident from DOS graph) that will ultimately lead to change its electro-optical properties. Furthermore, the HOMO-LUMO (H-L) orbital energy gap is found to be dependent on the number of states per interval of energy originating from picrate anion and can be tuned by modifying the picrate anion fragment according to DOS diagram. Thus, the picrate anion plays a crucial role to tune the optical and nonlinear optical properties of LALAPM.

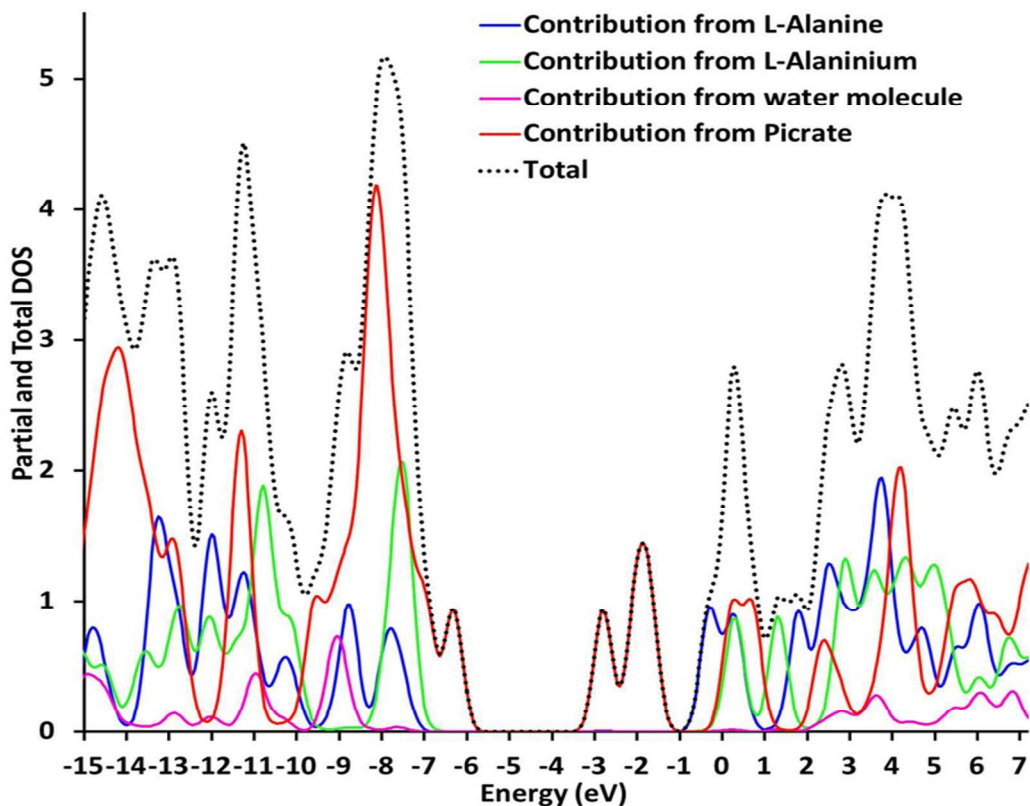


**Figure 9** Total density of state (TDOS) and partial density of state (PDOS) plots for LALAPM molecule.

### 3.3.5. Diffuse reflectance study

The diffuse reflectance of the titled crystal has been measured as shown in Figure 10(a) and evaluated its band gap. The diffuse reflectance is a destructive method for surface measurements using a mirror like reflection from the surface of the sample. Generally the Kubelka-Munk theory is used for diffuse reflectance spectra analysis from the weakly absorbing samples. In such a case the Kubelka-Munk equation at any wavelength is given by:

$$F(R) = \frac{(1-R)^2}{2R} \quad (6)$$

Where  $R$  is the absolute reflectance of the sample and  $F(R)$  is called Kubelka-Munk function. For this measurement, we have powdered our grown crystals very finely and load into the sample holder and the recorded DR spectra is shown in the Figure 10(a).

The equation (6) can be written in terms of  $F(R)$  as follows:

$$\alpha = \frac{\text{absorbance}}{t} = \frac{F(R)}{t} \quad (7)$$

where the symbols are having their usual meanings and the value of  $t$  of the loaded circular sample is 0.5 mm. To determine the optical band gap of the sample using diffuse reflectance data the equation (7) can be written as:

$$\alpha h\nu = \frac{F(R)h\nu}{t} = A(h\nu - E_g)^{\frac{1}{n}} \quad (8)$$

where the symbols are having their usual meanings. The band gap was found to be 2.64 and 4.4 e.V calculated by the same procedure as mentioned above and the graph between  $h\nu$  vs  $[F(R)h\nu/t]^2$  is shown in Figure 10(b). The optical band gap calculated from UV-vis-NIR data was found to be almost similar to the diffuse reflectance.

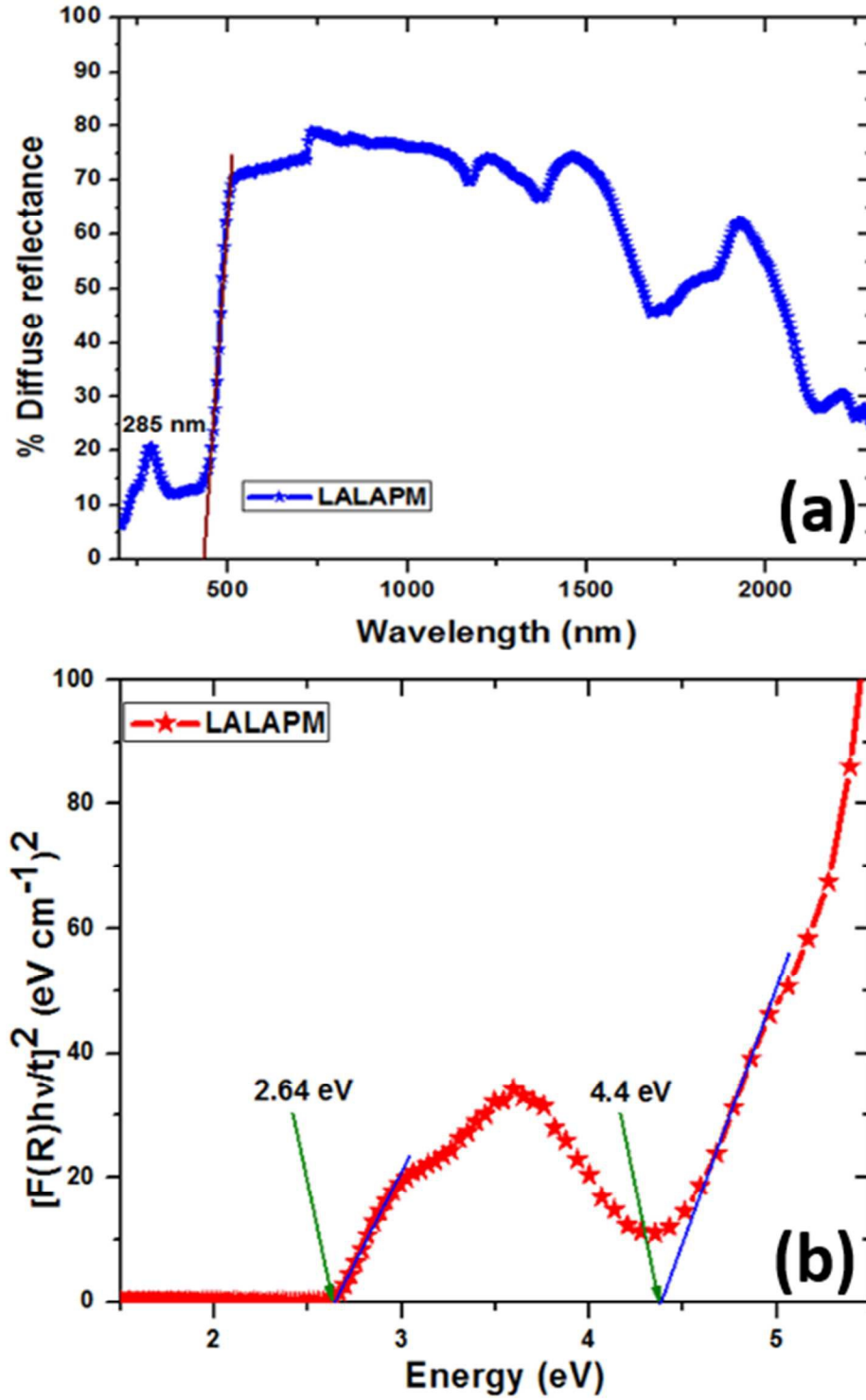


**Figure 10** (a) Diffuse reflectance spectrum and (b) optical band gap plots of LALAPM.

### 3.4. Polarizability and First hyperpolarizability

In our present investigation, we have calculated the electronic dipole moment ( $\mu$ ), molecular polarizability and first hyperpolarizability. For a molecule, its  $\mu$  is defined as follows:

$$\mu = \left( \mu_x^2 + \mu_y^2 + \mu_z^2 \right)^{1/2} \quad (9)$$

The average polarizability ( $\alpha_0$ ) can be calculated by following equations:

$$\alpha_0 = \frac{1}{3} (\alpha_{xx} + \alpha_{yy} + \alpha_{zz}) \quad (10)$$

For anisotropy of polarizability ( $\Delta\alpha$ )

$$\Delta\alpha = \frac{1}{\sqrt{2}} \sqrt{[(\alpha_{xx} - \alpha_{yy})^2 + (\alpha_{yy} - \alpha_{zz})^2 + (\alpha_{zz} - \alpha_{xx})^2 + 6\alpha_{xz}^2]} \quad (11)$$

Similarly, the magnitude of the first static hyperpolarizability ( $\beta_0$ ) can also be calculated using following eq.

$$\beta_0 = \left( \beta_x + \beta_y + \beta_z \right)^{1/2}, \quad (12)$$

where

$$\beta_i = \frac{3}{5} \sum_j \beta_{ijj}, \quad (j = x, y, z) \quad (13)$$

The second-order polarizability ( $\beta$ ) is a third rank tensor that can be described by a  $3 \times 3 \times 3$  matrix. According to Kleinman symmetry ( $\beta_{xyy} = \beta_{yxy} = \beta_{yyx}$ ,  $\beta_{yyz} = \beta_{zyy} = \beta_{zzy}$ ,... likewise other permutations also take same value), the 27 components of the 3D matrix can be reduced to 10 components.<sup>69</sup> The details of 10 components have been shown in Table 5. It is well acknowledged fact that the importance of polarizability and hyperpolarizability of a molecular

system is dependent on the electronic communication of two different parts of a molecule. The calculated values of dipole moment (a. u.), average polarizability ( $\alpha_0$ ), anisotropy of polarizability ( $\Delta\alpha$ ) and hyperpolarizability ( $\beta$ ) are given in Table 5.

**Table 5** The calculated values of polarizability ( $\alpha$ ), hyperpolarizability ( $\beta$ ) and dipole moment ( $\mu$ ) along their individual tensor components for LALAPM

Components	a. u.	( $\times 10^{-24}$ ) esu	Component	a. u.	( $\times 10^{-30}$ ) esu
$\alpha_{xx}$	139	20.60	$\beta_{xxx}$	-10	-0.09
$\alpha_{xy}$	8	1.19	$\beta_{xyy}$	-24	-0.21
$\alpha_{yy}$	267	39.56	$\beta_{xzz}$	-181	-1.56
$\alpha_{xz}$	-14	-2.07	$\beta_{xxy}$	-952	-8.23
$\alpha_{yz}$	-5	-0.74	$\beta_{yyy}$	22	0.19
$\alpha_{zz}$	262	38.82	$\beta_{yzz}$	79	0.68
$\alpha_0$	222	32.99	$\beta_{xxz}$	670	5.79
$\Delta\alpha$	384	56.90	$\beta_{yyz}$	22	0.19
$\mu_x$	1.174	2.98 <sup>a</sup>	$\beta_{zzz}$	61	0.53
$\mu_y$	0.249	0.63D	$\beta_{xxx}$	-622	-5.37
$\mu_z$	-4.006	-10.18D	$\beta_{tot}$	933	8.06
$\mu_{tot}$	4.182	10.63D	$\beta_0$	559	4.84
$\mu_{tot}$ (Urea)	1.66	4.24D (4.56D) <sup>b</sup>	$\beta_0$ (Urea)	26	0.22

<sup>a</sup> Units of  $\mu$  in Debye (D), for  $\mu$ , 1 Debye (D) =  $1 \times 10^{-18}$  esu-cm,  $\alpha$ , 1 a. u. =  $0.1482 \times 10^{-24}$  esu, for  $\beta$ , 1 a. u. =  $0.008629 \times 10^{-30}$  esu, <sup>b</sup> Exp.<sup>70</sup>

The total  $\mu$  value for LALAPM molecule has been observed 10.63 D. The highest component of  $\mu$  is  $\mu_z$  having a value of -10.18 D. This clearly indicates that the  $\mu$  of LALAPM is entirely directed from picrate ion towards L-alanine L-alaninium dimer along the negative z-axis as shown in Figure 3. In the similarly way, the average polarizability ( $\alpha_0$ ), anisotropy of polarizability ( $\Delta\alpha$ ) and hyperpolarizability ( $\beta_{\text{tot}}$ ) of LALAPM molecule have non-zero values of  $32.99 \times 10^{-24}$ ,  $56.90 \times 10^{-24}$  and  $8.06 \times 10^{-30}$  esu., respectively. The non-zero value of  $\beta_{\text{tot}}$  shows that the titled molecule possesses microscopic first static hyperpolarizability. The first hyperpolarizability value of LALAPM molecule is 37 times larger than that of urea as calculated in present investigation at the same B3LYP/6-31G\* level of theory. Furthermore, a careful analysis of individual tensor components of  $\beta_{\text{tot}}$  amplitude indicates that the off-diagonal components ( $\beta_{xxz}, \beta_{xxy}$ ) have larger values as compared to its diagonal components. These larger off-diagonal components indicate good nonlinear anisotropy, which a ration ( $\eta$ ) between off-diagonal and diagonal components.<sup>71, 72</sup> The NLO chromophores with good nonlinear anisotropy ratios have several advantages (better phase matching and increased stability in the polar order in pole polymers) over tradition linear chromophores with donor- $\pi$ -conjugated-acceptor configurations.<sup>73</sup> Why the  $\beta$  amplitude of LALAPM is relatively larger than that of urea? To trace the origin of relative  $\beta$  amplitude of LALAPM, we considered the widely used two-level approximation.<sup>74-77</sup>

$$\beta = \frac{3}{2} \Delta\mu \times \frac{f_0}{\Delta E^3} \quad (14)$$

where  $\Delta\mu$ , and are change in dipole moment from ground to excited state,  $f_0$  is oscillator strength and  $\Delta E$  is the transition energy. According to two-level approximation, the third power of

transition energy is inversely proportional to the  $\beta$  amplitude. The transition energy can be considered as decisive factor to determine the  $\beta$  amplitude. From Table 6, it can be seen that the transition energy of LALAM is significantly lower than that of urea. Thus according to two-level approximation, it is reasonable that the  $\beta$  amplitude of LALAPM is several times larger than that of urea molecule.

**Table 6.** The Transition energy  $\Delta E$ , oscillator strength ( $f_0$ ) change in dipole moment from ground to excited state ( $\Delta\mu$ ) and static hyperpolarizability ( $\beta_0$ ) as calculated at B3LYP/6-31G\* level of theory

Systems	$\Delta E$ (eV)	$f_0$	$\Delta\mu$ (Debye)	$\beta_0$ (a. u.)
LALAPM	2.996	0.133	0.813	559
Urea	7.902	0.001	2.383	26

### 3.4.1. Frequency Dependent Polarizability and First Hyperpolarizability

In addition to static first hyperpolarizability values, we have also calculated the dynamic (frequency dependent) electric field induced SHG (EFISHG) first hyperpolarizabilities ( $\beta_\omega$  and  $\mu\beta$ ), which are usually approximated as complement to the experimental first hyperpolarizability values. The frequency dependent coupled-perturbed Kohn-Sham (CPKS) method with the B3LYP functional has been applied to calculate the dynamic first hyperpolarizability values. In case of EFISHG experiments, the measurement provide information on the projection of the vector part of  $\beta$  on the dipole moment vectors as given by following Eq.

$$\beta_\omega(-2\omega; \omega, \omega) = \beta_\omega = \frac{3}{5} \sum_{\zeta}^{x,y,z} \frac{\mu_\zeta \beta_\zeta}{\|\mu\|} \quad (15)$$

where  $\mu$  is the norm of dipole moment vector and  $\mu_\zeta$  and  $\beta_\zeta$  are the components of  $\mu$  and  $\beta$  vectors. The product of first hyperpolarizability and dipole moment vectors ( $\mu\beta_\omega$ ) can be finally calculated using following relationship:

$$\mu\beta_\omega = \frac{5}{3} \mu \cdot \beta_\omega \quad (16)$$

All the  $\mu\beta_\omega$  values have been given in electrostatic units ( $10^{-48}$  esu) within T-convention of reference.<sup>78</sup> In CPKS method, the matrices of CPKS equation are expanded in Taylor series of external dynamic electric field and are solved analytically order by order. According to experimental setup for EFISHG first hyperpolarizability ( $\mu\beta_\omega$ ) measurement, the frequency dependent calculations are carried out using different optical wavelengths. We have calculated the dynamic frequency dependent values of polarizability including isotropic polarizability and anisotropic polarizability as well as the first hyperpolarizability ( $\mu\beta_\omega$ ) for LALAPM. The dynamic frequency dependent values of first hyperpolarizability are complementary to the experimental values that are determined using electric field induced second harmonic generation (EFISHG) technique (dynamic frequency dependent first hyperpolarizability). A number of laser frequency values have been used to determine the effect of frequency on  $\mu\beta_\omega$  values. In present investigation, a number of optical wavelengths have been used to determine the effect of incident laser wavelengths on polarizabilities ( $\alpha_{\text{iso}}$ , and  $\alpha_{\text{iso}}$ ),  $\beta_\omega$  and  $\mu\beta_\omega$  values.

**Table 7.** The calculated values of frequency dependent polarizabilities including isotropic and anisotropic polarizability along with dynamic EFISHG hyperpolarizability ( $\beta_\omega$ , in  $\times 10^{-30}$  esu) and the product  $\mu\beta_\omega$  ( $\mu\beta = 5/3 \mu \cdot \beta_\omega$ , in  $\times 10^{-48}$  esu) for LALAPM

Frequency (nm)	$\alpha_{\text{iso}}$ ( $\times 10^{-24}$ esu)	$\alpha_{\text{aniso}}$ ( $\times 10^{-24}$ esu)	$\beta_\omega$ ( $\times 10^{-30}$ esu)	$\mu\beta_\omega$ ( $\times 10^{-48}$ esu)
487	44.48	33.88	22.45	490.14
543.7	41.51	29.27	18.59	405.81
632.8	39.46	26.33	14.89	325.25
799.4	37.92	24.23	11.92	260.35
1064	37.03	23.62	10.24	223.56
1064 (Urea)	4.05	4.51	0.173 (0.45) <sup>a</sup>	1.228

<sup>a</sup> Experimental SHG value of Urea as calculated at  $\omega = 1064$  nm in water.<sup>70</sup>

From Table 7, it can be seen that for polarizability both its isotropic and anisotropic values show a gradual increase with decreasing the optical wavelengths of laser. A similar trend can also be seen for all the frequency dependent EFISHG values. The  $\beta_\omega$  values are also found to be larger than static first hyperpolarizability ( $\beta_0$ ). The  $\beta_\omega$  and  $\mu\beta_\omega$  hyperpolarizabilities show a gradual increase in their amplitudes with a decrease in optical wavelengths. The five different optical wavelengths have been used in present investigation, ranging from the lowest 487 nm to the highest 1064 nm. The frequency dependent  $\beta_\omega$  value for urea molecule has also been calculated at the same level of theory that is often used as a standard NLO molecule. The frequency dependent  $\beta_\omega$  value of urea molecule has been found to be  $0.173 \times 10^{-30}$  esu that is slightly underestimated as compared to its experimental SHG value  $0.45 \times 10^{-30}$  esu in water at 1064 nm. According to some previous computational studies, this underestimation is due to improper solvent effects.<sup>79</sup> A comparison between LALAPM and urea  $\beta_\omega$  values show that LALAPM has

about 59 times larger than that of urea. The different frequency dependent values of  $\beta_\omega$  and  $\mu\beta_\omega$  have been plotted over a range of wavelengths that shows the frequency dependent hyperpolarizabilities gradually increase towards lower wavelengths or higher frequency of incident laser. The graphical representation of frequency dependent hyperpolarizabilities ( $\beta_\omega$  and  $\mu\beta_\omega$ ) with different wavelengths is shown in Figure 11.

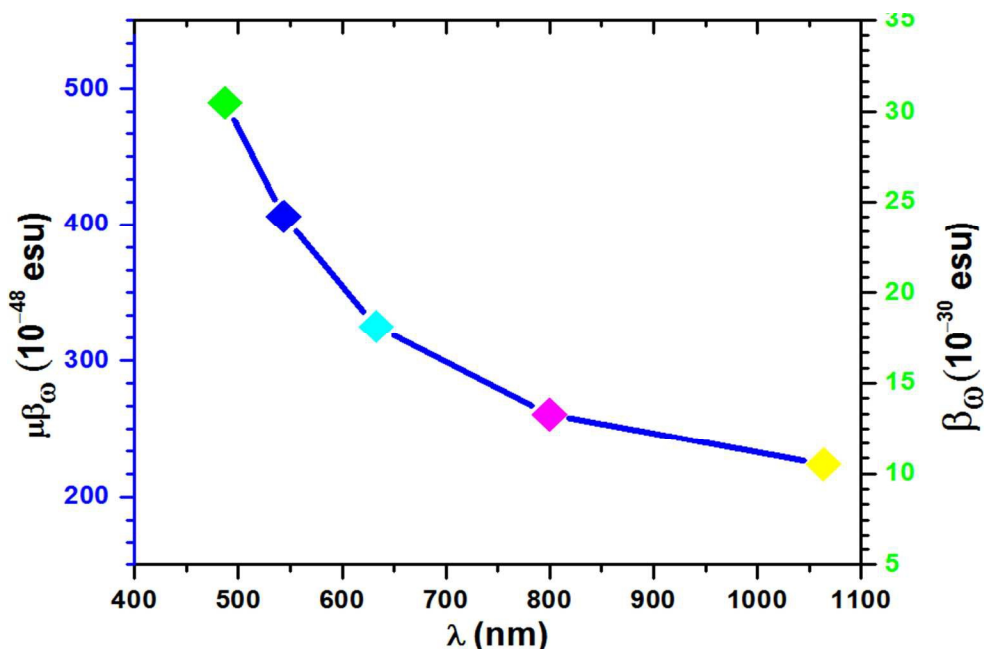
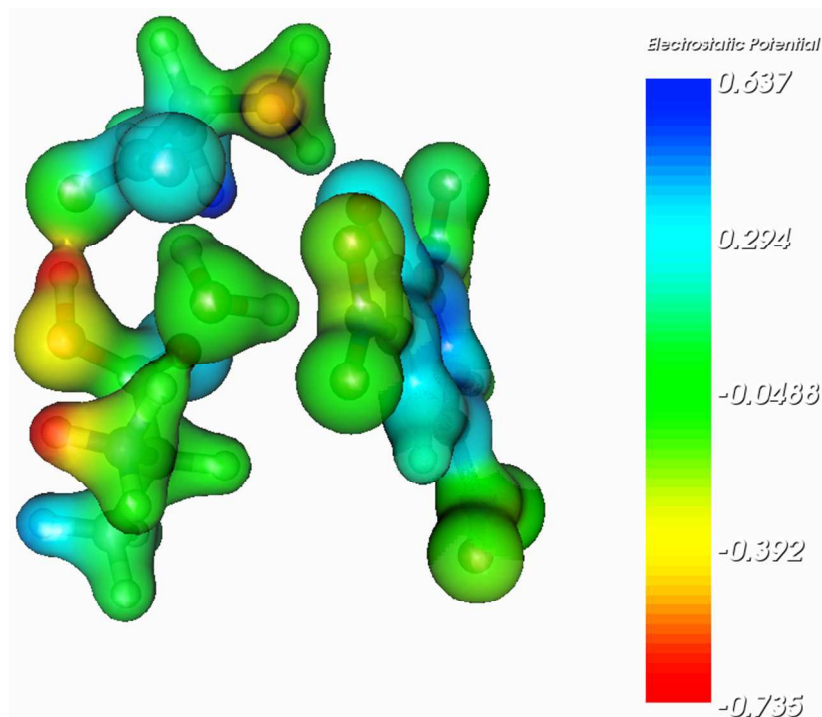


Figure 11. The graphical representation of frequency dependent hyperpolarizabilities ( $\beta_\omega$  and  $\mu\beta_\omega$ ) with different wavelengths

### 3.5. Molecular Electrostatic Potential (MEP)

To have molecular level understanding, we have calculated 3-D plots of molecular electrostatic potential (MEP) of LALAPM molecule as shown in Figure 12. The MEP is the measurement of electrostatic potential on constant electron density surface. The 3-D plots of MEP surface overlap on the top of total energy density. The MEP is helpful property to investigate the reactivity of molecular species by predicted that either the approaching nucleophile is attracted to a positive region of molecule. In MEP plot, while maximum positive region that is preferred site for

nucleophilic attack indicated as blue color. Similarly, a maximum negative region is preferred site for electrophilic attack that is indicated as red surface. The MEP of LALAPM has been drawn in Figure 12 to get simultaneous information about its molecular size, shape along with its positive, negative and neutral electrostatic potential regions in terms of color grading.



**Figure 12** Molecular electrostatic potential (MEP) plot of LALAPM molecule with iso-value 0.0400 a. u.

A careful analysis of Figure 11 provides important information about LALAPM structure-property relationship. For instance, the maximum positive potential regions are phenyl ring of picrate anion, H-atoms of methyl groups of L-alanine and L-alaninium. The positive potential of phenyl group is perhaps due to the three strongly withdrawing  $\text{NO}_2$  groups, which have significantly attracted the electron density making phenyl ring susceptible to external nucleophiles. On the other hand, the important negative potential regions are H-atoms of  $\text{NH}_3$  and COOH groups as well as three  $\text{NO}_2$  groups of phenyl ring. Unlike the H atoms of  $\text{NH}_3$  and

COOH groups, the negative potential of NO<sub>2</sub> groups are delocalized equally on all three atoms of each NO<sub>2</sub> group. The sites with positive and negative potentials on LALAPM molecule also provide the information about intermolecular and intramolecular hydrogen bonds (between different colors) mainly including O<sub>13</sub>...H<sub>14</sub>, O<sub>27</sub>...H<sub>25</sub> and O<sub>15</sub>...H<sub>46</sub> etc. Using MEP, the relative polarity can also be understood for LALAPM molecule. For example, the dimer of L-alanine and L-alaninium shows localized negative potential sites on left side (red color) while phenyl ring has delocalized positive potential (blue color) over whole ring resulting in larger molecular polarity, which can lead to significant solvatochromism with external dielectric environment as well as larger polarizabilities by interacting with external electric fields.

#### 4. Conclusion

We have successfully applied the dual approach comprising of experimental and computational techniques to investigate the LALAPM. The single crystals of L-alanine L-alaninium picrate monohydrate (LALAPM) were grown successfully by slow cooling technique for the first time. The crystal morphology was recorded during its growth, which found to vary confirming the different type of crystal formations i.e. L-alanine and LALAPM. The grown crystals were subjected to single crystal, powder X-ray diffraction analyses to confirm its structure. The obtained lattice parameters from single crystal XRD as well as refined parameter from powder XRD data are found in close agreement with the reported values. Additionally, the grown crystals were cut and polished for ultraviolet-visible-near infrared and diffuse reflectance measurement using optical parameter analyses. The optical transmission spectrum showed that the grown crystals are highly transparent in the entire testing range. The lower cut-off wavelength of LA was observed at ~230 nm while for LALAPM two cut-off wavelengths were observed at ~286 and ~435 nm respectively. The diffuse reflectance spectra showed one

absorption band at ~285 nm similar to transmission spectra. Two optical band gaps were found for LALAPM, i.e., ~2.86, ~4.68 eV and ~2.64, ~4.4 eV, calculated from absorbance data and diffuse reflectance data respectively, which are very close to each other. Furthermore, using different computational methods, the ground state molecular geometry of LALAPM was optimized at B3LYP/6-31G\*, M06/6-31G\* and MP2/6-31G\* levels of theory. The structural, spectroscopic, linear and nonlinear optical properties were calculated and the obtained theoretical findings were compared with reported as well as our experimental results. The calculated values of static ( $\beta_{\text{tot}}$ ) and dynamic first hyperpolarizability ( $\beta_{\omega}$ ) of the titled compound were found to be 37 and 59 times larger than a typical prototype urea, respectively. The state of art calculations of molecular electrostatic potential, total and partial densities of states analyses provided several novel features of individual molecular components in LALAPM complex. The obtained results indicate that the titled compound is having good nonlinear optical properties and can be treated as a good contender for optoelectronic device fabrications as well.

### **Acknowledgement**

The authors are thankful to King Khalid University and Research Center for Advanced Materials Science (RCAMS), King Khalid University, Abha 61413, P.O. Box 9004, Saudi Arabia for providing research infrastructure.

## References

1. B. F. Levine and C. G. Bethea, *The Journal of Chemical Physics*, 1975, 63, 2666-2682.
2. S. Muhammad and M. Nakano, *Nanoscience and Computational Chemistry: Research Progress*, 2013, 309.
3. N. Zaitseva and L. Carman, *Progress in Crystal Growth and Characterization of Materials*, 2001, 43, 1-118.
4. M. Shkir, B. Riscob and G. Bhagavannarayana, *Solid State Sciences*, 2012, 14, 773-776.
5. M. Shkir and H. Abbas, *Spectrochimica Acta Part A: Molecular and Biomolecular Spectroscopy*, 2014, 118, 172-176.
6. G. Bhagavannarayana, B. Riscob and M. Shkir, *Materials Chemistry and Physics*, 2011, 126, 20-23.
7. J. Badan, R. Hierle, A. Perigaud, J. Zyss and D. Williams, 1993.
8. S. Muhammad, A. Irfan, M. Shkir, A. R. Chaudhry, A. Kalam, S. AlFaify, A. G. Al-Sehemi, A. Al-Salami, I. Yahia and H. L. Xu, *J. Comput. Chem.*, 2015, 36, 118-128.
9. S. Muhammad, *J. Mol. Graphics Modell.*, 2015, 59, 14-20.
10. M. Kitazawa, R. Higuchi, M. Takahashi, T. Wada and H. Sasabe, *Appl. Phys. Lett.*, 1994, 64, 2477-2479.
11. M. Shkir, S. AlFaify, H. Abbas and S. Muhammad, *Spectrochimica Acta Part A: Molecular and Biomolecular Spectroscopy*, 2015, 147, 84-92.
12. M. Shkir, S. Muhammad and S. AlFaify, *Spectrochimica Acta Part A: Molecular and Biomolecular Spectroscopy*, 2015, 143, 128-135.
13. M. N. Bhat and S. M. Dharmaprakash, *J. Cryst. Growth*, 2002, 236, 376-380.
14. J. Nicoud and R. Twieg, *Nonlinear optical properties of organic molecules and crystals*, 1987, 1, 227-296.
15. Y. In, H. Nagata, T. Ishida and A. Wakahara, *Acta Crystallogr. Sect. C: Cryst. Struct. Commun.*, 1997, 53, 367-369.
16. P. Zaderenko, M. S. Gil, P. López, P. Ballesteros, I. Fonseca and A. Albert, *Acta Crystallographica Section B*, 1997, 53, 961-967.
17. P. Srinivasan, T. Kanagasekaran, R. Gopalakrishnan, G. Bhagavannarayana and P. Ramasamy, *Crystal growth & design*, 2006, 6, 1663-1670.

18. M. Shakir, S. Kushwaha, K. Maurya, M. Arora and G. Bhagavannarayana, *Journal of crystal growth*, 2009, 311, 3871-3875.
19. M. Shakir, B. Singh, B. Kumar and G. Bhagavannarayana, *Applied Physics Letters*, 2009, 95, 252902-252902-252903.
20. Mohd. Shakir, G. Bhagavannarayana, B. K. Singh and Binay Kumar, *NPG Asia Materials*, 2010.
21. S.-i. Yamaguchi, M. Goto, H. Takayanagi and H. Ogura, *Bull. Chem. Soc. Jpn.*, 1988, 61, 1026-1028.
22. L. Koreneva, V. Zolin and B. Davydov, *Molecular crystals in nonlinear optics*, Nauka, Moscow, Russian, 1975.
23. J. Baran, A. J. Barnes and H. Ratajczak, *Spectrochimica Acta Part A: Molecular and Biomolecular Spectroscopy*, 1995, 51, 197-214.
24. L. Misoguti, A. Varela, F. Nunes, V. Bagnato, F. Melo, J. Mendes Filho and S. Zilio, *Opt. Mater.*, 1996, 6, 147-152.
25. S. Boomadevi and K. Pandiyan, *Physica B: Condensed Matter*, 2014, 432, 67-70.
26. V. V. Ghazaryan, M. Fleck and A. M. Petrosyan, *Spectrochimica Acta Part A: Molecular and Biomolecular Spectroscopy*, 2011, 78, 128-132.
27. K. Anitha, S. Athimoolam and R. Rajaram, *Acta Crystallographica Section E: Structure Reports Online*, 2005, 61, 1604-1606.
28. K. Anitha, B. Sridhar and R. Rajaram, *Acta Crystallogr. Sect. Sect. E: Struct. Rep. Online*, 2004, 60, o1530-o1532.
29. M. Sivaramkumar, R. Velmurugan, M. Sekar, P. Ramesh and M. Ponnuswamy, *Acta Crystallogr. Sect. Sect. E: Struct. Rep. Online*, 2010, 66, o1821-o1821.
30. K. Anitha and R. K. Rajaram, *Acta Crystallographica Section E*, 2005, 61, o589-o591.
31. K. Anitha, S. Athimoolam and R. K. Rajaram, *Acta Crystallographica Section E*, 2006, 62, o8-o10.
32. M. Briget Mary, V. Sasirekha and V. Ramakrishnan, *Spectrochimica Acta Part A: Molecular and Biomolecular Spectroscopy*, 2006, 65, 414-420.
33. M. B. Mary, V. Sasirekha and V. Ramakrishnan, *Spectrochimica Acta Part A: Molecular and Biomolecular Spectroscopy*, 2006, 65, 955-963.

34. K. Anitha, S. Annavenus, B. Sridhar and R. K. Rajaram, *Acta Crystallographica Section E*, 2004, 60, o1722-o1724.
35. V. Ghazaryan, M. Fleck and A. Petrosyan, 2010.
36. V. Ghazaryan, M. Fleck and A. Petrosyan, *Journal of Molecular Structure*, 2012, 1015, 51-55.
37. T. Freeda, T. Vela and P. Selvarajan, *Journal of Experimental Sciences*, 2010, 1.
38. D. Shanthi, P. Selvarajan and R. J. Mani, *Optik-International Journal for Light and Electron Optics*, 2014, 125, 2531-2537.
39. M. Shkir, S. Alfaify, M. Ajmal Khan, E. Dieguez and J. Perles, *Journal of Crystal Growth*, 2014, 391, 104-110.
40. D. Lechuga-Ballesteros and N. Rodriguez-Hornedo, *Pharm. Res.*, 1993, 10, 1008-1014.
41. C. Razzetti, M. Ardoino, L. Zanotti, M. Zha and C. Paorici, *Cryst. Res. Technol.*, 2002, 37, 456-465.
42. V. V. Ghazaryan, M. Fleck and A. M. Petrosyan, *J. Mol. Struct.*, 2012, 1015, 51-55.
43. M. J. Frisch, G. W. Trucks, H. B. Schlegel, G. E. Scuseria, M. A. Robb, J. R. Cheeseman, G. Scalmani, V. Barone, B. Mennucci and G. A. Petersson, *There is no corresponding record for this reference.*
44. S. Muhammad, H. Xu, M. R. S. A. Janjua, Z. Su and M. Nadeem, *PCCP*, 2010, 12, 4791-4799.
45. T. Koopmans, *Physica*, 1933, 1, 104-113.
46. R. G. Parr and P. K. Chattaraj, *Journal of the American Chemical Society*, 1991, 113, 1854-1855.
47. R. G. Pearson, *J. Am. Chem. Soc.*, 1986, 108, 6109-6114.
48. R. G. Parr and R. G. Pearson, *Journal of the American Chemical Society*, 1983, 105, 7512-7516.
49. V. Bisker-Leib and M. F. Doherty, *Crystal growth & design*, 2003, 3, 221-237.
50. M. Shkir, B. Riscob, V. Ganesh, N. Vijayan, R. Gupta, J. Plaza, E. Dieguez and G. Bhagavannarayana, *Journal of Crystal Growth*, 2013, 380, 228-235.
51. A. Teimouri, A. N. Chermahini, K. Taban and H. A. Dabbagh, *Spectrochimica Acta Part A: Molecular and Biomolecular Spectroscopy*, 2009, 72, 369-377.

52. B. Riscob, M. Shakir, J. Kalyana Sundar, S. Natarajan, M. Wahab and G. Bhagavannarayana, *Spectrochimica Acta Part A: Molecular and Biomolecular Spectroscopy*, 2011, 78, 543-548.
53. M. Shkir, B. Riscob, M. Hasmuddin, P. Singh, V. Ganesh, M. Wahab, E. Dieguez and G. Bhagavannarayana, *Optical Materials*, 2014, 36, 675-681.
54. M. L. Caroline, M. Prakash, D. Geetha and S. Vasudevan, *Spectrochimica Acta Part A: Molecular and Biomolecular Spectroscopy*, 2011, 79, 1936-1940.
55. M. L. Caroline and S. Vasudevan, *Mater. Lett.*, 2008, 62, 2245-2248.
56. A. L. Rose, P. Selvarajan and S. Perumal, *Mater. Chem. Phys.*, 2011, 130, 950-955.
57. D. R. Babu, D. Jayaraman, R. M. Kumar and R. Jayavel, *Journal of crystal growth*, 2002, 245, 121-125.
58. M. Shkir, S. Muhammad, S. AlFaify, A. Irfan and I. Yahia, *Spectrochimica Acta Part A: Molecular and Biomolecular Spectroscopy*, 2015, 137, 432-441.
59. M. Shkir, H. Abbas, S. Kumar, G. Bhagavannarayana and S. AlFaify, *Journal of Physics and Chemistry of Solids*, 2014, 75, 959-965.
60. M. Shkir, S. Muhammad and S. AlFaify, *Spectrochimica Acta Part A: Molecular and Biomolecular Spectroscopy*, 2015.
61. M. Shkir, S. AlFaify, H. Abbas and G. Bhagavannarayana, *Materials Chemistry and Physics*, 2015.
62. D. Jacquemin, J. Preat and E. A. Perpète, *Chemical Physics Letters*, 2005, 410, 254-259.
63. D. Jacquemin, J. Preat, M. Charlot, V. Wathélet, J.-M. André and E. A. Perpète, *The Journal of chemical physics*, 2004, 121, 1736-1743.
64. M. Cossi and V. Barone, *The Journal of Chemical Physics*, 2001, 115, 4708-4717.
65. M. Shakir, B. Riscob, K. Maurya, V. Ganesh, M. Wahab and G. Bhagavannarayana, *Journal of Crystal Growth*, 2010, 312, 3171-3177.
66. M. Shakir, S. Kushawaha, K. Maurya, S. Kumar, M. Wahab and G. Bhagavannarayana, *Journal of Applied Crystallography*, 2010, 43, 491-497.
67. M. Shakir, S. Kushwaha, K. Maurya, G. Bhagavannarayana and M. Wahab, *Solid State Communications*, 2009, 149, 2047-2049.
68. S. I. Gorelsky and A. B. P. Lever, *J. Organomet. Chem.*, 2001, 635, 187-196.
69. D. Kleinman, *Physical Review*, 1962, 126, 1977.

70. I. Ledoux and J. Zyss, *Chem. Phys.*, 1982, 73, 203-213.
71. S. Muhammad, M. R. S. A. Janjua and Z. Su, *The Journal of Physical Chemistry C*, 2009, 113, 12551-12557.
72. S. Muhammad, H. Xu, Z. Su, K. Fukuda, R. Kishi, Y. Shigeta and M. Nakano, *Dalton Transactions*, 2013, 42, 15053-15062.
73. M. A. Ramírez, A. M. Cuadro, J. Alvarez-Builla, O. Castaño, J. L. Andrés, F. Mendicuti, K. Clays, I. Asselberghs and J. J. Vaquero, *Organic & biomolecular chemistry*, 2012, 10, 1659-1669.
74. J. L. Oudar and D. S. Chemla, *The Journal of Chemical Physics*, 1977, 66, 2664-2668.
75. S. Muhammad, H. Xu, Y. Liao, Y. Kan and Z. Su, *J. Am. Chem. Soc.*, 2009, 131, 11833-11840.
76. S. Muhammad, H. Xu and Z. Su, *The Journal of Physical Chemistry A*, 2011, 115, 923-931.
77. S. Muhammad, T. Minami, H. Fukui, K. Yoneda, R. Kishi, Y. Shigeta and M. Nakano, *The Journal of Physical Chemistry A*, 2012, 116, 1417-1424.
78. A. Willetts, J. E. Rice, D. M. Burland and D. P. Shelton, *The Journal of Chemical Physics*, 1992, 97, 7590-7599.
79. A. Alparone and S. Millefiori, *Chem. Phys. Lett.*, 2005, 416, 282-288.